Synthesis and fluorescence and electrochemical properties of D–π-A structural isomers of benzofuro[2,3-*c*]oxazolo[4,5-*a*]carbazole-type and benzofuro[2,3-*c*]oxazolo[5,4-*a*]carbazole-type fluorescent dyes

Yousuke Ooyama, Genta Ito, Kohei Kushimoto, Kenji Komaguchi, Ichiro Imae and Yutaka Harima*

Received 25th February 2010, Accepted 1st April 2010
First published as an Advance Article on the web 29th April 2010
DOI: 10.1039/c003526b

Heteropolycyclic donor–π-acceptor (D–π-A) structural isomers of benzofuro[2,3-*c*]oxazolo[4,5-*a*]carbazole-type (**2a–f**) and benzofuro[2,3-*c*]oxazolo[5,4-*a*]carbazole-type fluorescent dyes (**3a–f**), which differ in the position of oxygen and nitrogen atoms of the oxazole ring, have been synthesized, and their photophysical and electrochemical properties have been investigated. The fluorescent dyes **2a–f** exhibit much stronger intramolecular charge transfer (ICT) absorption and fluorescence bands than **3a–f**. Both of the D–π-A structural isomers showed bathochromic shifts of the fluorescence band and a decrease in the fluorescence quantum yields with increasing solvent polarity (*i.e.*, positive fluorescence solvatochromism), and the bathochromic shifts for **3a–f** were larger than those for **2a–f**. The fluorescent dyes **2a–c** and **3a–c**, which have cyano and carboxyl groups, and carboxylic acid ester as electron-withdrawing substituents, exhibited significant fluorescence solvatochromic properties, compared to **2e**, **2f**, **3e** and **3f** without an electron-withdrawing substituent. The fluorescence solvatochromism of the fluorescent dyes were analyzed with the Lippert–Mataga correlation. Moreover, to elucidate the differences of photophysical properties among the fluorescent dyes, we have performed time-resolved fluorescence spectroscopic measurements, and a change of the electronic or molecular structures between the ground and excited states was evaluated by a comparison of the experimental radiative rate constant (k_r) with the Strickler–Berg rate constant (k_r^{SB}). The electrochemical properties of **2a–f** and **3a–f** were determined by cyclic voltammetry, which demonstrated that these fluorescent dyes have similar HOMO energy levels, but different LUMO energy levels. Semi-empirical molecular orbital calculations (AM1 and INDO/S) have been carried out to elucidate the effects of the substituents and chromophore skeleton on photophysical properties of the two D–π-A structural isomers. These studies indicated that the ICT characteristics in the excited state are different among the fluorescent dyes, which is a principal reason for the differences of the fluorescence solvatochromism and the substituent dependent fluorescence properties among the two D–π-A structural isomers.

Introduction

Donor–acceptor π-conjugated (D–π-A) fluorescent dyes with both electron-donating and electron-accepting groups linked by a π-conjugated bridge are useful as sensitizers of dye-sensitized solar cells (DSSCs),[1,2] emitters of organic light emitting diodes (OLEDs),[3] and fluorescence sensors in a variety of applications,[4] because of their strong absorption and emission properties originating from the intramolecular charge transfer (ICT) excitation from the donor to acceptor moiety of the D–π-A dyes. One of the noteworthy structural features of D–π-A dyes is that the electron density of the highest occupied molecular orbital (HOMO) is localized over the π-conjugated system close to the donor part, and that of the lowest unoccupied molecular orbital (LUMO) is localized over the acceptor part.[5] In light of the concept of the D–π-A structure, the increase in the electron-donating and electron-accepting abilities of donors (D) and acceptors (A), respectively, leads to the decrease in the energy gap between the HOMO and LUMO. Thus, the photophysical, electrochemical, and their related ICT properties of the D–π-A dyes strongly depend on the electron-donating ability of D and electron-accepting ability of A, as well as the electronic characteristics of the π bridge (chromophore). Moreover, the electron distribution on the D–π-A dye can be drastically changed upon excitation. This leads to a large change of dipole moment in the excited state and to considerable solvent polarity dependent fluorescence properties (*i.e.*, fluorescence solvatochromism)[5,6] so that they would be strategically tuned through the chemical modification of each constitutional unit (D, A, or π bridge) to suit the requirements for optoelectronic devices, and optical, biochemical and medicinal sensors.[1–4] However, there are few fundamental researches on the ICT characteristics of heteropolycyclic D–π-A fluorescent dyes.

In our previous study,[7] the heteropolycyclic D–π-A structural isomers of benzofuro[2,3-*c*]oxazolo[4,5-*a*]carbazole-type (**2a**) and benzofuro[2,3-*c*]oxazolo[5,4-*a*]carbazole-type fluorophores (**3a**) having dibutylamino group as D and cyano group as A, which differ only in the positions of oxygen and nitrogen atoms of

Department of Applied Chemistry, Graduate School of Engineering, Hiroshima University, Higashi-hiroshima, 739-8527, Japan. E-mail: harima@mls.ias.hiroshima-u.ac.jp; Fax: (+81) 82-424-5494

the oxazole ring, have been synthesized, and their photophysical properties in solution have been investigated (Scheme 1). Considerable differences in the absorption and fluorescence spectra were observed between the two structural isomers. The fluorophore **2a** exhibited much stronger ICT absorption and fluorescence bands than the fluorophore **3a**. Moreover, both the D–π-A structural isomers showed bathochromic shifts of the fluorescence band and a decrease in the fluorescence quantum yields (Φ) with increasing solvent polarity (*i.e.*, positive fluorescence solvatochromism). The bathochromic shifts and the degree of decrease in Φ for **3a** were larger than those for **2a**, so that the Stokes shift for **3a** was large compared to that for **2a**. It was suggested that the D–π-A structural isomers have a marked difference in degree of the donor–acceptor conjugation leading to the quite different absorption and fluorescence spectra in solution.

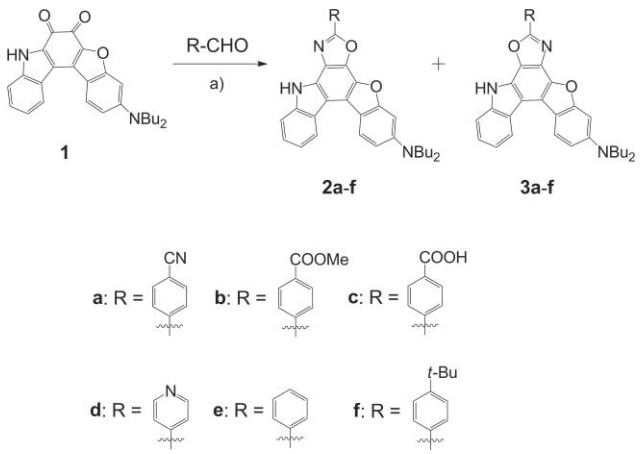

Scheme 1 Synthesis of fluorophores **2a–f** and **3a–f**. (a) CH_3COOH, CH_3COONH_4, 90 °C, 1–2 h; yields: 55% for **2a**, 16% for **3a**, 58% for **2b**, 29% for **3b**, 33% for **2c**, 5% for **3c**, 31% for **2d**, 12% for **3d**, 52% for **2e**, 17% for **3e**, 26% for **2f**, and 7% for **3f**.

In this work, to get a better understanding of the influences of electron-accepting groups and π-conjugation system on the photophysical properties related to ICT characteristics of the heteropolycyclic D–π-A fluorescent dyes, we have newly synthesized D–π-A structural isomers of benzofuro[2,3-*c*]oxazolo[4,5-*a*]carbazole-type (**2b–f**) and benzofuro[2,3-*c*]oxazolo[5,4-*a*]carbazole-type fluorescent dyes (**3b–f**) with dibutylamino group as D and different *p*-substituted phenyl groups as A, and their photophysical and electrochemical properties have been investigated. The fluorescence solvatochromism of the fluorescent dyes were analyzed with the Lippert–Mataga correlation. To elucidate the differences of photophysical properties among the fluorescent dyes, we have performed time-resolved fluorescence spectroscopic measurements, and a change of the electronic or molecular structures between the ground and excited states was evaluated by comparing the experimental radiative rate constant (k_r) with the Strickler–Berg rate constant (k_r^{SB}). The electrochemical properties of **2a–f** and **3a–f** were also determined by cyclic voltammetry (CV). Furthermore, semi-empirical molecular orbital calculations (AM1 and INDO/S) have been carried out to elucidate the effects of the substituents and chromophore skeleton on photophysical properties of the two D–π-A structural isomers. On the basis of the results of calculations and the spectral analyses, the influences of electron-accepting groups and π-conjugation system on the photophysical properties related to ICT characteristics of the heteropolycyclic D–π-A fluorescent dyes **2a–f** and **3a–f** are discussed.

Results and discussion

Synthesis of heteropolycyclic D–π-A structural isomers 2a–f and 3a–f

As shown in Scheme 1, we used 3-dibutylamino-8*H*-5-oxa-8-aza-indeno[2,1-*c*]fluorene-6,7-dione (**1**)[7] as a starting material. The quinone **1** was allowed to react with the corresponding arylaldehydes (4-*tert*-butylbenzaldehyde, benzaldehyde, 4-pyridinecarboxaldehyde, methyl 4-formylbenzoate, 4-formylbenzoic acid, and 4-formylbenzonitrile) to give the D–π-A structural isomers of benzofuro[2,3-*c*]oxazolo[4,5-*a*]carbazole-type (**2a–f**) and benzofuro[2,3-*c*]oxazolo[5,4-*a*]carbazole-type fluorescent dyes (**3a–f**), under conditions using ammonium acetate. In this reaction, NH_3 resulting from CH_3COONH_4 in the initial stage is acting as the nucleophilic reagent to the 6- and/or 7-carbonyl carbon. In this case, NH_3 preferentially attacks the 7-carbonyl carbon rather than the 6-carbonyl in spite of a similar steric reactivity of the two carbonyls. It was considered that the conjugated linkage of the dibutylamino group to the 6-carbonyl group would make the 6-carbonyl carbon less electrophilic than the 7-carbonyl carbon, so that the nucleophilic reagents (NH_3) preferentially attack the electrophilic 7-carbonyl carbon. As the result, this reaction afforded preferentially the compounds **2a–f**. These compounds were completely characterized by ^{1}H NMR, IR, and elemental analysis. A comparison of the observed and calculated UV-Vis spectra for **2a–f** and **3a–f** has provided powerful evidence for identification of the isomers, which will be described later on.

Absorption spectra of 2a–f and 3a–f in solution

The absorption spectral data of **2a–f** and **3a–f** in various solvents are summarized in Table 1. In cyclohexane, all compounds exhibit vibronic-structured absorption bands. In other solvents the absorption band is broadened and the vibronic structure is lost. The absorption spectra are nearly independent of solvent polarity (Fig. 1 and 2). This indicates that the electronic and structural characteristics of the ground and Franck–Condon (FC) excited states do not differ much with a change in solvent polarity. The compounds **2a–f** show two absorption maxima: one band occurs at around 340 nm ascribed to π→π* transition, and another band occurs at around 390–430 nm assigned to the ICT excitation from the donor (D) (dibutylamino group) to the acceptor (A) (*p*-substituted phenyl group). The ICT bands of **2a–f** in 1,4-dioxane show bathochromic shifts in the order of **2f** (387 nm) ≤ **2e** (388 nm) < **2d** (409 nm) < **2c** (416 nm) < **2b** (418 nm) < **2a** (428 nm) (Fig. 3a). The ICT bands are red-shifted by 21 nm for **2d**, 28 nm for **2c**, 30 nm for **2b**, and 40 nm for **2a** compared to the ICT band of the unsubstituted **2e** (Ph). Thus, the red-shifts of ICT band indicate that the electron-accepting abilities of *p*-substituted phenyl groups increase in the order of **2d** (4-Py) < **2c** (*p*-COOH-Ph) < **2b** (*p*-COOMe-Ph) < **2a** (*p*-CN-Ph). On the other

Table 1 Absorption and fluorescence spectral data of **2a–f** and **3a–f** in various solvents

Compound	Solvent	Absorption λ_{max}/nm (ε_{max}/M^{-1} cm^{-1})	$\int\varepsilon(\nu_a)d\nu_a/\nu_a$/$M^{-1}cm^{-1}$	Fluorescence λ_{max}/nm	Stokes shift ν_{st}/cm^{-1}
2a	Cyclohexane	460 (—), 431 (—), 410 (—), 348 (—)[a]	—[a]	505, 472	3400
	1,4-Dioxane	428 (25 900), 350 (27 300)	1.07×10^8	539	4812
	THF	429 (24 100), 350 (27 100)	1.01×10^8	582	6128
	Acetone	427 (24 700), 349 (26 200)	1.04×10^8	617	7212
2b	Cyclohexane	447 (—), 421 (—), 400 (—), 344 (—)[a]	—[a]	491, 460	3386
	1,4-Dioxane	418 (25 800), 348 (27 100)	1.21×10^8	532	5126
	THF	421 (25 400), 349 (27 900)	1.20×10^8	565	6054
	Acetone	415 (26 900), 349 (27 200)	1.33×10^8	605	7567
2c	Cyclohexane	—[a]	—[a]	—[a]	—[a]
	1,4-Dioxane	416 (24 300), 347 (24 000)	1.17×10^8	526	5027
	THF	416 (23 700), 347 (23 600)	1.14×10^8	547	5757
	Acetone	407 (23 500), 347 (22 100)	1.26×10^8	603	7986
2d	Cyclohexane	434 (—), 408 (—), 373 (—), 342 (—)[a]	—[a]	472, 445	3323
	1,4-Dioxane	409 (23 400), 348 (23 400)	1.22×10^8	511	4880
	THF	411 (24 500), 346 (25 600)	1.25×10^8	536	5674
	Acetone	406 (24 100), 344 (23 000)	1.22×10^8	592	7739
2e	Cyclohexane	408 (—), 386 (—), 370 (—)[sh], 335 (—)[a]	—[a]	443, 421	3333
	1,4-Dioxane	388 (32 900), 338 (21 400)	1.33×10^8	463	4175
	THF	389 (32 800), 338 (21 900)	1.30×10^8	485	5088
	Acetone	387 (35 200), 337 (21 200)	1.44×10^8	506	6077
2f	Cyclohexane	406 (17 500), 384 (26 200) 365 (21 700), 334 (18 100)	1.24×10^8	440, 415	3314
	1,4-Dioxane	387 (31 000), 335 (17 700)	1.30×10^8	455	3795
	THF	388 (30 100), 338 (17 900)	1.34×10^8	471	4542
	Acetone	387 (28 600), 337 (15 500)	1.29×10^8	497	5719
3a	Cyclohexane	442 (—), 390 (—), 360 (—)[a]	—[a]	513, 484	3131
	1,4-Dioxane	430 (4700), 390[sh], 359 (60 200)	0.15×10^8	575	5865
	THF	430 (5900), 390[sh], 359 (69 200)	0.19×10^8	623	7204
	Acetone	430 (5600), 390[sh], 357 (72 000)	0.18×10^8	531	4423
3b	Cyclohexane	438 (—), 390 (—), 357 (—)[a]	—[a]	501, 470	2871
	1,4-Dioxane	430 (4100), 390[sh], 359 (62 100)	0.13×10^8	562	5462
	THF	430 (4100), 390[sh], 358 (58 700)	0.13×10^8	608	6808
	Acetone	430 (3800), 390[sh], 357 (60 600)	0.12×10^8	525	4208
3c	Cyclohexane	—[a]	—[a]	—[a]	—[a]
	1,4-Dioxane	430 (3700), 388[sh], 358 (51 200)	0.12×10^8	551	5107
	THF	430 (3500), 388[sh], 357 (50 500)	0.11×10^8	560	5399
	Acetone	430 (2900), 388[sh], 353 (51 100)	0.10×10^8	524	4172
3d	Cyclohexane	407 (—), 371 (—), 353 (—)[a]	—[a]	487, 458	4036
	1,4-Dioxane	413 (5500), 380[sh], 354 (38 800)	0.19×10^8	547	5932
	THF	413 (5000), 380[sh], 355 (36 800)	0.17×10^8	568	6607
	Acetone	413 (5900), 380[sh], 355 (37 600)	0.19×10^8	503	4332
3e	Cyclohexane	386 (—), 346 (—), 336 (—)[a]	—[a]	446, 425	3485
	1,4-Dioxane	388 (7700), 338 (43 300)	0.18×10^8	494	5530
	THF	388 (7600), 338 (44 800)	0.18×10^8	510	6165
	Acetone	388 (7700), 336 (43 700)	0.17×10^8	542	7323
3f	Cyclohexane	385 (4900), 348 (27 300), 335 (30 300)	0.16×10^8	445, 420	3502
	1,4-Dioxane	387 (5200), 338 (30 300)	0.16×10^8	487	5306
	THF	387 (5100), 338 (31 000)	0.16×10^8	497	5719
	Acetone	387 (5100), 335 (30 500)	0.16×10^8	522	6683

[a] Poor solubility.

hand, for **3a–f**, the band ascribed to π→π* transition appeared at around 340 nm, and a feeble and broad ICT band was observed at around 380–430 nm (Fig. 3c). For **3a–3d**, a shoulder band was observed at around 390 nm. Similarly to **2a–f**, the red-shifts of ICT band are dependent on the electron-accepting abilities of *p*-substituted phenyl groups. Consequently, the π→π* transition for **3a–f** is stronger than that for **2a–f**, while the ICT excitation for **2a–f** is stronger than that for **3a–f**. These results suggest that an increase in the ICT characteristics leads to a decrease in π→π* transitions, so that the degree of donor–acceptor conjugation for **2a–f** is larger than that for **3a–f** owing to the conjugated linkage of the dibutylamino group to *p*-substituted phenyl group in **2a–f**.

Fluorescence spectra of 2a–f and 3a–f in solution

The fluorescent spectral data of **2a–f** and **3a–f** in various solvents are summarized in Table 2. In cyclohexane, all the compounds exhibit vibronic-structured fluorescence bands, while in other solvents the fluorescence bands are broad with no vibronic structures. The fluorescence maxima of both **2a–f** and **3a–f** in 1,4-dioxane show bathochromic shifts in the order of **2f**, **3f** (455 nm, 487 nm) ≤ **2e**, **3e** (463 nm, 494 nm) < **2d**, **3d** (511 nm, 547 nm) < **2c**, **3c** (526 nm, 551 nm) < **2b**, **3b** (532 nm, 562 nm) < **2a**, **3a** (539 nm, 575 nm), with increasing the electron-accepting ability of *p*-substituted phenyl group (Fig. 3b and d). The fluorescence maxima are red-shifted by 48 nm for **2d**, 63 nm for **2c**, 69 nm for **2b**, and

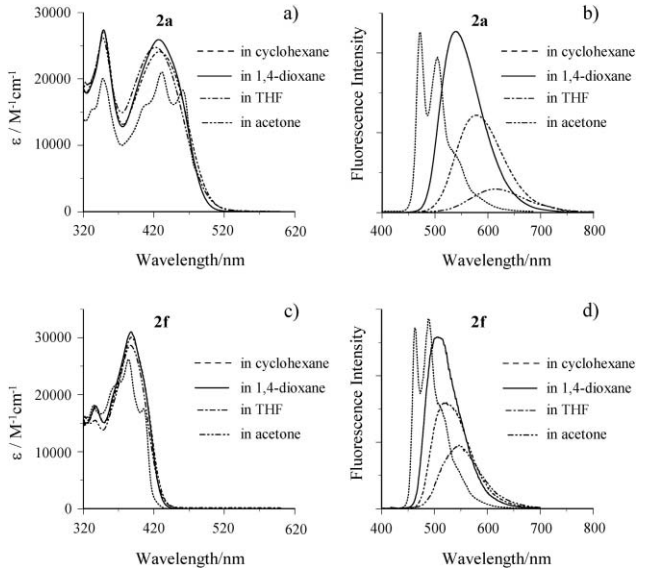

Fig. 1 (a) Absorption and (b) fluorescence spectra of **2a** in cyclohexane, 1,4-dioxane, THF, and acetone, and (c) absorption and (d) fluorescence spectra of **2f** in cyclohexane, 1,4-dioxane, THF, and acetone. Absorption and fluorescence spectra of **2a** in cyclohexane are enlarged because of poor solubility of **2a**.

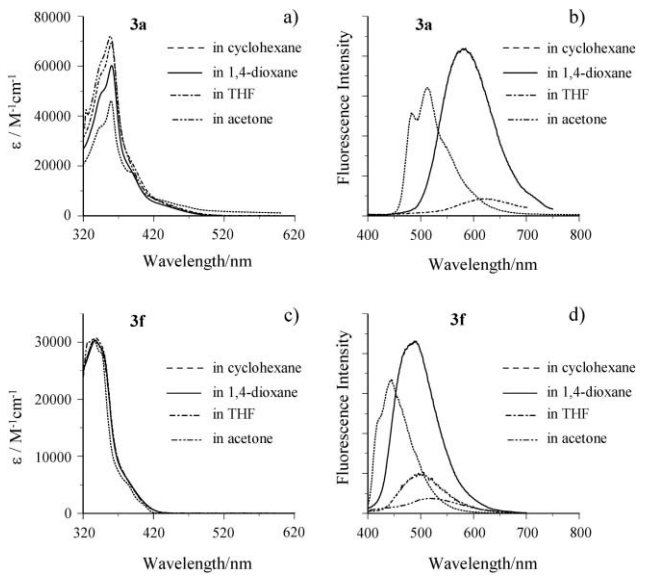

Fig. 2 (a) Absorption and (b) fluorescence spectra of **3a** in cyclohexane, 1,4-dioxane, THF, and acetone, and (c) absorption and (d) fluorescence spectra of **3f** in cyclohexane, 1,4-dioxane, THF, and acetone. Absorption and fluorescence spectra of **3a** in cyclohexane are enlarged because of poor solubility of **3a**.

76 nm for **2a** relative to the fluorescence maximum of unsubstituted **2e** (Ph), and by 53 nm for **3d**, 57 nm for **3c**, 68 nm for **3b**, and 81 nm for **3a** relative to the fluorescence maximum of the unsubstituted **3e** (Ph). In contrast to the absorption spectra, the fluorescence spectra are strongly dependent on solvent polarity. The fluorescence maxima of **2a–f**, **3e**, and **3f** show a large bathochromic shift on increasing the solvent polarity from cyclohexane to acetone. On the other hand, although the fluorescence maxima of **3a–d**, except **3c**, show a large bathochromic shift on increasing the solvent

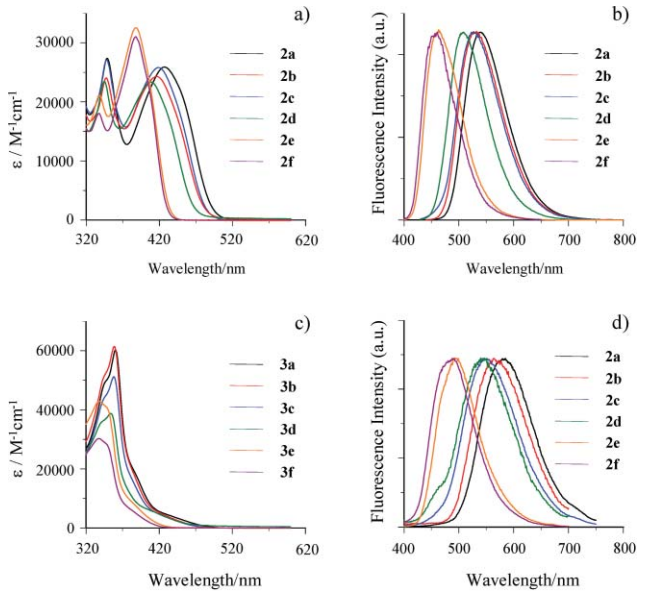

Fig. 3 (a) Absorption and (b) fluorescence spectra of **2a–f** in 1,4-dioxane, and (c) absorption and (d) fluorescence spectra of **3a–f** in 1,4-dioxane.

polarity from cyclohexane to 1,4-dioxane, in turn, the fluorescence maxima of **3a–d** show a hypsochromic shift in acetone (Table 2, Fig. 1 and 2). However, except in acetone, the Stokes shift values for **2a–f** and **3a–f** are very large in polar solvents. More interestingly, the solvent polarity-dependent Stokes shift values increased with increasing of the electron-accepting ability of *p*-substituted phenyl groups, and the Stokes shift values for **3a–f** are large compared to those for **2a–f**. The substituent-dependent fluorescence properties and the fluorescence solvatochromism are illustrated by photos in Fig. 4.

Solvent-dependent shifts in the fluorescence maxima of D–π-A fluorescent dyes can be mainly attributed to the dipole–dipole interactions between fluorescent dye and solvent molecules.[6,8] Thus, in order to get an insight into the fluorescence solvatochromisms of **2a–f** and **3a–f**, the relationships between the solvent polarity dependent fluorescence spectra and the dipole moments of fluorophores were investigated on the basis of the Lippert–Mataga equation [eqn (1)]:[5b,6,9]

$$\nu_{st} = \frac{1}{4\pi\varepsilon_0}\cdot\frac{2\Delta\mu^2}{hca^3}\Delta f + \text{Const.} \quad (1)$$

where

$$\Delta f = \frac{\varepsilon - 1}{2\varepsilon + 1} - \frac{n^2 - 1}{2n^2 + 1} \quad (2)$$

$$a = \left(\frac{3M}{4\pi d N_a}\right)^{1/3} \quad (3)$$

In the above equations, ν_{st} is the Stokes shift, ε_0 is the vacuum permittivity, h is Planck's constant, c is the velocity of light, a is the Onsager radius of fluorophore, $\Delta\mu = \mu_e - \mu_g$ is the difference in the dipole moment of fluorophore between the excited (μ_e) and the ground (μ_g) states, ε and n are the static dielectronic constant and the refractive index of the solvent, respectively, Δf is the orientation polarizability, M is the molecular weight, d is

Table 2 Photophysical data of **2a–f** and **3a–f** in various solvents

Compound	Solvent	Φ_f	τ_f/ns	k_r/s	k_{nr}/s	k_{nr}/k_r	k_r^{SB}/s	k_r/k_r^{SB}
2a	Cyclohexane	0.78	3.15	2.48×10^8	0.70×10^8	0.28	—[a]	—[a]
	1,4-Dioxane	0.99	4.07	2.44×10^8	0.03×10^8	0.01	1.71×10^8	1.43
	THF	0.48	4.37	1.10×10^8	1.19×10^8	1.08	1.25×10^8	0.88
	Acetone	0.16	2.93	0.55×10^8	2.87×10^8	5.22	1.00×10^8	0.55
2b	Cyclohexane	0.70	2.87	2.44×10^8	1.05×10^8	0.43	—[a]	—[a]
	1,4-Dioxane	0.96	4.07	2.36×10^8	0.09×10^8	0.04	1.96×10^8	1.21
	THF	0.75	4.24	1.77×10^8	0.59×10^8	0.33	1.59×10^8	1.11
	Acetone	0.30	2.40	1.25×10^8	2.92×10^8	2.34	1.33×10^8	0.94
2c	Cyclohexane	—[a]	—[a]	—[a]	—[a]		—[a]	—[a]
	1,4-Dioxane	0.97	3.77	2.57×10^8	0.08×10^8	0.03	1.95×10^8	1.32
	THF	0.78	4.02	1.94×10^8	0.55×10^8	0.28	1.65×10^8	1.18
	Acetone	0.16	2.26	0.71×10^8	3.72×10^8	5.24	1.24×10^8	0.57
2d	Cyclohexane	0.81	2.74	2.95×10^8	0.69×10^8	0.23	—[a]	—[a]
	1,4-Dioxane	0.96	3.96	2.42×10^8	0.10×10^8	0.04	2.18×10^8	1.11
	THF	0.78	4.24	1.84×10^8	0.52×10^8	0.28	1.90×10^8	0.97
	Acetone	0.65	4.41	1.47×10^8	0.79×10^8	0.53	1.27×10^8	1.16
2e	Cyclohexane	0.84	2.21	3.80×10^8	0.72×10^8	0.19	—[a]	—[a]
	1,4-Dioxane	0.96	2.97	3.24×10^8	0.13×10^8	0.04	3.02×10^8	1.07
	THF	0.85	3.09	2.75×10^8	0.49×10^8	0.18	2.53×10^8	1.09
	Acetone	0.76	3.53	2.15×10^8	0.68×10^8	0.32	2.29×10^8	0.94
2f	Cyclohexane	0.74	2.03	3.64×10^8	1.28×10^8	0.35	3.27×10^8	1.11
	1,4-Dioxane	0.98	2.66	3.69×10^8	0.08×10^8	0.02	3.36×10^8	1.10
	THF	0.79	2.79	2.84×10^8	0.75×10^8	0.26	2.83×10^8	1.00
	Acetone	0.74	3.09	2.40×10^8	0.84×10^8	0.35	2.16×10^8	1.11
3a	Cyclohexane	0.30	8.38	0.36×10^8	0.84×10^8	2.33	—[a]	—[a]
	1,4-Dioxane	0.17	5.21	0.33×10^8	1.59×10^8	4.82	0.20×10^8	1.64
	THF	0.02	1.21	0.17×10^8	8.10×10^8	47.7	0.20×10^8	0.87
	Acetone	$\ll 0.02$	—[b]	—[b]	—[b]	2.33	—[b]	—[b]
3b	Cyclohexane	0.40	8.03	0.50×10^8	0.75×10^8	1.50	—[a]	—[a]
	1,4-Dioxane	0.14	5.34	0.26×10^8	1.61×10^8	6.19	0.19×10^8	1.52
	THF	0.02	1.14	0.18×10^8	8.60×10^8	47.8	0.15×10^8	1.24
	Acetone	$\ll 0.02$	—[b]	—[b]	—[b]		—[b]	—[b]
3c	Cyclohexane	—[a]	—[a]	—[a]	—[a]		—[a]	—[a]
	1,4-Dioxane	0.11	4.28	0.26×10^8	2.08×10^8	8.00	0.18×10^8	1.44
	THF	0.03	1.94	0.15×10^8	5.01×10^8	33.4	0.31×10^8	0.48
	Acetone	0.05	4.15	0.12×10^8	2.29×10^8	19.1	0.16×10^8	0.75
3d	Cyclohexane	0.30	7.57	0.40×10^8	0.92×10^8	2.30	—[a]	—[a]
	1,4-Dioxane	0.23	5.71	0.40×10^8	1.35×10^8	3.38	0.27×10^8	1.47
	THF	0.12	4.43	0.27×10^8	1.99×10^8	7.37	0.22×10^8	1.24
	Acetone	0.05	5.91	0.08×10^8	1.60×10^8	20.0	0.34×10^8	0.23
3e	Cyclohexane	0.23	4.78	0.48×10^8	1.61×10^8	3.35	—[a]	—[a]
	1,4-Dioxane	0.34	8.76	0.39×10^8	0.75×10^8	1.92	0.34×10^8	1.15
	THF	0.23	8.76	0.26×10^8	0.88×10^8	3.39	0.29×10^8	0.89
	Acetone	0.13	6.01	0.22×10^8	1.45×10^8	6.59	0.22×10^8	0.99
3f	Cyclohexane	0.23	4.61	0.50×10^8	1.67×10^8	3.34	0.41×10^8	1.22
	1,4-Dioxane	0.33	7.91	0.42×10^8	0.85×10^8	2.02	0.32×10^8	1.33
	THF	0.18	7.08	0.25×10^8	1.16×10^8	4.64	0.29×10^8	0.86
	Acetone	0.07	5.00	0.14×10^8	1.90×10^8	13.6	0.23×10^8	0.61

[a] Poor solubility. [b] Too weak.

the density of molecule, and N_a is Avogadro's number. Therefore, based on eqn (1), the change in dipole moment, $\Delta\mu = \mu_e - \mu_g$, can simply be estimated from the slope of a plot of ν_{st} against Δf.

The Lippert–Mataga plots for **2a–f** and **3a–f** are shown in Fig. 5. The plots for **2a–f** are reasonably linear, suggesting that dipole–dipole interactions between the fluorophore and solvent are mainly responsible for the solvent-dependent fluorescent shift. The slopes (m_{sl}) for **2a–c** are steeper than those for **2e** and **2f**. The steep slopes show that the fluorescence properties are significantly dependent on the solvent polarity. The Onsager radius of fluorophore (a) and ground state dipole moment (μ_g) are listed in Table 3, together with the excited dipole moments (μ_e) evaluated from the slopes (m_{sl}) of the Lippert–Mataga plots and μ_g values. The values of μ_e increase in the order of **2e** (5.69 D) < **2f** (5.83 D) < **2d** (8.42 D) < **2a** (10.30 D) < **2b** (11.33 D) < **2c** (12.01 D), which is nearly comparable to the increase of the electron-accepting abilities of *p*-substituted phenyl groups. The very large values of μ_e for **2a–c** having the stronger electron-withdrawing groups indicate significant ICT characteristics in the excited state, so that the fluorescence maxima of **2a–c** are strongly dependent on the solvent polarity. Therefore, the increasing of solvent polarity stabilizes the ICT excited state relative to the ground state, resulting in large bathochromic shifts of fluorescence maximum. In contrast to **2a–f**, no linear correlation can be seen for **3a–d**. It was inferred that because of the less donor–acceptor conjugation from the dibutylamino group to *p*-substituted phenyl group, no linear correlation for **3a–d** can be seen between Δf and the Stokes shift.

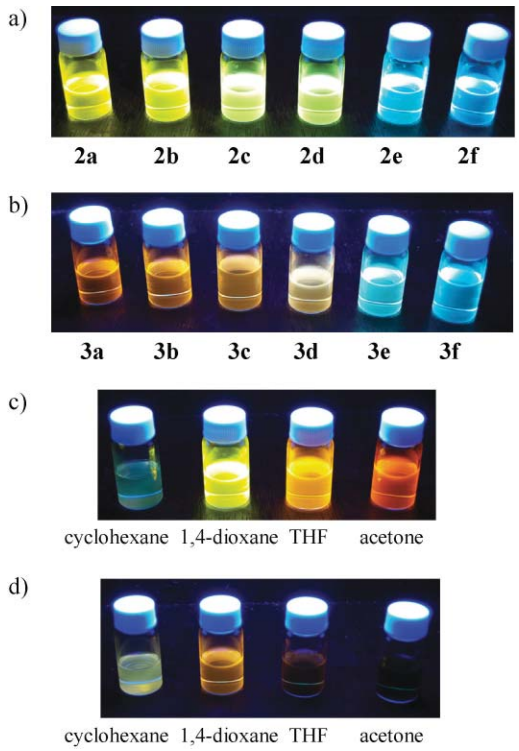

Fig. 4 Fluorescence images of (a) **2a–f** and (b) **3a–f** in 1,4-dioxane. Fluorescence solvatochromism of (c) **2a** and (d) **3a** in cyclohexane, 1,4-dioxane, THF, and acetone.

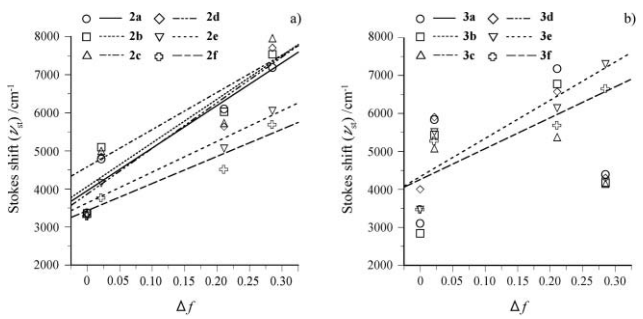

Fig. 5 Correlation of the Stokes shift and the Lippert–Mataga polarity parameter according to eqn (1) and (2) for (a) **2a–f** and (b) **3a–f**.

Table 3 Onsager radius (a) and ground state dipole moments (μ_g) and excited state dipole moments (μ_e), and slope (m_{sl}) of Lippert–Mataga plots for **2a–f**, **3e**, and **3f**

Compound	a/Å[a]	m_{sl} / cm^{-1}[b]	μ_g/D[c]	μ_e/D
2a	5.94	11 194	5.21	10.30
2b	6.05	11 486	6.03	11.33
2c	6.00	9786	7.18	12.01
2d	5.84	12 000	3.28	8.42
2e	5.84	8088	1.47	5.69
2f	6.05	7129	1.65	5.83
3e	5.84	10 049	1.84	6.54
3f	6.05	8125	2.42	6.88

[a] Onsager radius calculated by eqn (3) with $d = 1.0$ g cm^{-3}. [b] Calculated from Lippert–Mataga plots. [c] Obtained from semi-empirical MO calculations.

Fluorescence quantum yields and time-resolved fluorescence studies

The fluorescence quantum yields (Φ_f) and lifetimes (τ_f) of **2a–f** and **3a–f** were measured in several solvents. The radiative ($k_r = \Phi_f/\tau_f$) and nonradiative ($k_{nr} = (1 - \Phi_f)/\tau_f$) rate constants were calculated by using the Φ_f and τ_f values. The values of Φ_f, τ_f, k_r, and k_{nr} are given in Table 2. In all the solvents used, the Φ values of **2a–f** are greater than those of **3a–f**. The time-resolved fluorescence spectroscopy of **2a–f** and **3a–f** indicated that the radiative rate constants (k_r) for **2a–f** are larger than those for **3a–f**; in contrast, the nonradiative rate constants (k_{nr}) for **3a–f** are larger than those for **2a–f**. The ratios of nonradiative constant to radiative constant (k_{nr}/k_r) for **3a–f** are larger than those for **2a–f**, suggesting that the non-radiative decay in **3a–f** is accelerated. Therefore, the higher Φ values of **2a–f** are mainly due to the large k_r and the small k_{nr} values compared to those of **3a–f**, which may attribute to that the degree of donor–acceptor conjugation for **2a–f** is larger than that for **3a–f** owing to the conjugated linkage of the dibutylamino group to *p*-substituted phenyl group in **2a–f**. Significant dependence of the values of Φ_f, τ_f, k_r, and k_{nr} on the solvent polarity was also observed. For **2a** and **2b**, the Φ and τ_f values increase from cyclohexane to 1,4-dioxane, and then significantly decrease with increasing polarity from 1,4-dioxane to acetone. The k_r values for **2a–c** decrease with increasing polarity from cyclohexane to acetone. On the other hand, the Φ and k_r values for **2d–f** increase also from cyclohexane to 1,4-dioxane, and then slightly decrease with increasing polarity from 1,4-dioxane to acetone. As the polarity increases from cyclohexane to acetone, the τ_f values for **2d–f** slightly increase. For **3a–c**, the Φ_f, τ_f, and k_r values significantly decrease with increasing polarity from cyclohexane to acetone, compared to the cases of **2a–c**. The Φ_f, τ_f, and k_r values for **3d** gradually decrease with increasing solvent polarity. On the other hand, the τ_f and Φ values for **3e** and **3f** increase with increasing polarity from cyclohexane to 1,4-dioxane, and then gradually decrease with increasing polarity from 1,4-dioxane to acetone. The k_r values for **3e** and **3f** decrease with increasing polarity from cyclohexane to acetone. These results indicate that the Φ_f, τ_f, and k_r values for both **2a–c** and **3a–c** with the stronger electron-withdrawing substituents significantly decreased with increasing solvent polarity, compared to the cases of **2e**, **2f**, **3e**, and **3f** without electron-withdrawing substituents.

In order to investigate whether the variations of fluorescence quantum yields and lifetimes for **2a–f** and **3a–f** with changing of the solvent and the *p*-substituted phenyl groups attribute to the differences of the electronic or molecular structures between the ground and the excited states, we used the Strickler–Berg (S–B) equation, which allowed us to estimate the radiative rate constant k_r^{SB} from the absorption and fluorescence spectra [eqn (4)]:[5a,10]

$$k_r^{SB} = \frac{8\pi c 10^3 \ln 10}{N_a} n^2 \nu_f^3 \int \frac{\varepsilon(\nu_a)d\nu_a}{\nu_a} \quad (4)$$

where ν_f is the wavenumber of fluorescence maximum and $\varepsilon(\nu_a)$ is the molar extinction coefficient at wavelength ν_a. In general, good agreements between the experimental radiative rate constant k_r and the radiative rate constant k_r^{SB} calculated from the S–B relation were obtained, indicating that the electronic or molecular structure in the excited state is the same as in the ground state.[5a,8,11] It was difficult to estimate the values of k_r^{SB} for **2a–e** and **3a–e** in cyclohexane, because of their poor solubilities. The k_r/k_r^{SB} values

for **2d–f** were very close to unity and similar in all the solvents used, which indicates that the structural differences between the absorbing and emitting states are very small for **2d–f** in all the solvents used. Although the k_r/k_r^{SB} values for **3e** and **3f** were also close to unity, the larger solvent polarity, the larger is the deviation from $k_r/k_r^{SB} = 1$. On the other hand, in the cases of **2a–c** and **3a–d**, the k_r/k_r^{SB} values are not equal to unity in polar solvents, implying that the excitation also leads to significant changes in the molecular and electronic structure of **2a–c** and **3a–d**. The deviations from $k_r/k_r^{SB} = 1$ for **3a–d** are larger than those for **2a–c**, indicating significant changes in the molecular and electronic structure of **3a–d** in the excited state. Moreover, the k_r/k_r^{SB} values differ considerably among the used solvents, suggesting that the excited state structure for **2a–c** and **3a–d** varies with the solvents.

ICT characteristics of D–π-A structural isomers 2a–f and 3a–f

On the basis of the Lippert–Mataga and the Strickler–Berg relations, we will discuss photophysical properties of **2a–f** and **3a–f** below. In non-polar solvents such as cyclohexane, the Φ_f values for **2a–f** and **3a–f** are low, suggesting that non-radiative decay is accelerated by an inter-system crossing (ISC) channel leading to the formation of a triplet state (T_1), as shown in Fig. 6. The ICT state, which is attributed to partial charge transfer from donor to acceptor groups in the excited state, is formed only in very small amounts in cyclohexane, because the ICT state is unlikely to be stabilized in non-polar solvents.

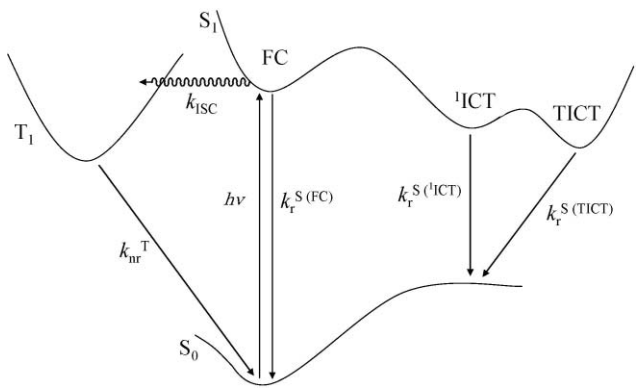

Fig. 6 Energy diagram for **2a–f** and **3a–f**.

For the cases of **2a–c** with the stronger electron-withdrawing substituents, in 1,4-dioxane, the ^{1}ICT state is formed in high yield, leading to an increase in Φ_f and τ_f values (Fig. 6). With further increase in solvent polarity, the Φ_f and τ_f values drastically decrease. The k_r/k_r^{SB} values are not equal to 1, suggesting that the excitation leads to significant changes in the molecular or electronic structures of **2a–c**. Gopidas *et al.* have reported that for the donor–acceptor-substituted tetrahydropyrene with cyano and nitro groups as acceptor groups, in highly polar solvents the Φ_f and τ_f values are very low and this is attributed to a deactivation pathway involving the twisting of the nitro group with respect to the phenyl ring of tetrahydropyrene to which it is attached.[5a,8] Thus, the twisted intramolecular charge transfer (TICT) state, which is attributed to full charge transfer from donor to acceptor groups in the excited state, is induced by the twisting which leads to non-radiative deactivation and reduces Φ_f and τ_f values. They concluded that a strong electron-withdrawing group such as nitro can stabilize a negative charge in the excited state, and the TICT state by twisting of the nitro group is a predominant excited state deactivation pathway in polar solvents. On the other hand, with weaker acceptor groups such as acetyl, this pathway is not important at all. In our case, therefore, for **2a–c** bearing cyano and carboxyl groups and carboxylic acid ester as the stronger electron-withdrawing group, in polar solvent such as acetone, the predominant species in the excited state is the TICT state, which is responsible for the twisting between the *p*-substituted phenyl groups and the benzofuro[2,3-*c*]oxazolocarbazole moiety. Thus, we conclude that the decreases of Φ_f, τ_f, and k_r values in polar solvents are owing to the TICT state. In the TICT state, the localized charges on the electron-withdrawing substituents are stabilized better in polar solvents, which reduces the energy of the excited states (S_1) further, leading to a large bathochromic shift of fluorescence maxima on increasing the solvent polarity from 1,4-dioxane to acetone. The decreases of Φ_f, τ_f, and k_r values for **3a–d** with increasing solvent polarity are larger than those for **2a–c**, which attributed to the predominant TICT state for **3a–d**, due to the larger twist between the *p*-substituted phenyl groups and the benzofuro[2,3-*c*]oxazolocarbazole moiety. It was found that the deviation from $k_r/k_r^{SB} = 1$ for **3c** are larger than those for **3a** and **3b**, indicating that the significant changes in the molecular and electronic structure of **3c** occurred in the excited state, because of specific solvent-dye interaction such as hydrogen bonding or the dissociation and the intramolecular proton transfer of the carboxyl proton in the excited state. Also, the low Φ_f values and the hypochromic shift of fluorescence maxima for **3a–d** in acetone may attribute to the changes in the molecular and electronic structure by the rotation of the *p*-substituted phenyl groups. On the other hand, the k_r/k_r^{SB} values for **2e** and **2f** without electron-withdrawing substituent were very close to unity. This suggests that the molecular structural changes are very small, so that the TICT state is not at all important. Therefore, the ^{1}ICT state for **2e** and **2f** is stabilized in polar solvents, which is responsible for the relatively high Φ_f and τ_f values in polar solvents. The k_r/k_r^{SB} values for **3e** and **3f** were close to unity compared to the values for **3a–c**, suggesting that the predominant species for **3e** and **3f** in the excited state is the ^{1}ICT state.

Consequently, we found that with the increase in solvent polarity, the predominant excited state for the D–π-A fluorescent dyes (**2a–c** and **3a-c**) with the stronger electron-withdrawing groups change from the ^{1}ICT state to the TICT state, and the less donor–acceptor π-conjugated D–π-A fluorescent dyes (**3a–f**) prefer the TICT state to the ^{1}ICT state, compared to the more donor–acceptor π-conjugated D-π-A fluorescent dyes (**2a–f**).

Electrochemical properties

The electrochemical properties of **2a–f** and **3a–f** were determined by CV in acetonitrile for **2a**, **2e**, **2f**, **3a**, **3e**, and **3f** and DMF for **2b–d** and **3b–d** containing 0.1 M Et_4NClO_4. As an example, the CVs of **2e** and **3e** are shown in Fig. 7. The CV data are summarized in Table 4. The first oxidation peaks for **2a–f** and **3a–f** were determined to be 0.31–0.43 V *vs.* Ag/Ag^+. The corresponding reduction peaks appeared at 0.25-0.35 V. The first redox waves are clearly observed and the peak separations are *ca.* 50–80 mV, suggesting that the first oxidized states of the dyes are stable. On

Table 4 Electrochemical properties of **2a–f** and **3a–f** in acetonitrile

Compound	$E_{pa}{}^{ox}$/V[a]	$E_{pc}{}^{ox}$/V[a]	ΔE_p/mV	$E_{1/2}$/V
2a	0.36, 0.87, 1.00	0.29, 0.82, 0.93	70, 50, 70	0.33, 0.85, 0.97
2b	0.38, 0.87, 0.99	0.31, 0.81, —	70, 60, —	0.35, 0.84, —
2c	0.31, 0.82, 0.98	0.25, —, —	60, —, —	0.28, —, —
2d	0.43, 1.04, —	0.36, —, —	70, —, —	0.40, —, —
2e	0.37, 0.89, —	0.29, 0.79, —	80, 100, —	0.33, 0.84, —
2f	0.35, 0.83, —	0.29, 0.77, —	60, 60, —	0.32, 0.80, —
3a	0.33, 0.88, 1.01	0.26, 0.82, 0.96	70, 60, 50	0.30, 0.85, 0.99
3b	0.38, 0.91, 1.04	0.31, 0.84, —	70, 70, —	0.35, 0.88, —
3c	0.33, 0.68, —	0.27, —, —	60, —, —	0.30, —, —
3d	0.40, 0.64, —	0.35, —, —	50, —, —	0.38, —, —
3e	0.37, 0.91, 1.02	0.29, 0.84, —	80, 70, —	0.33, 0.88, —
3f	0.36, 0.93, —	0.29, 0.82, —	70, 100, —	0.33, 0.88, —

[a] E_{pa} and E_{pc} are the anodic and cathodic peak potentials. Potentials are all referred to Ag/Ag^+ in acetonitrile.

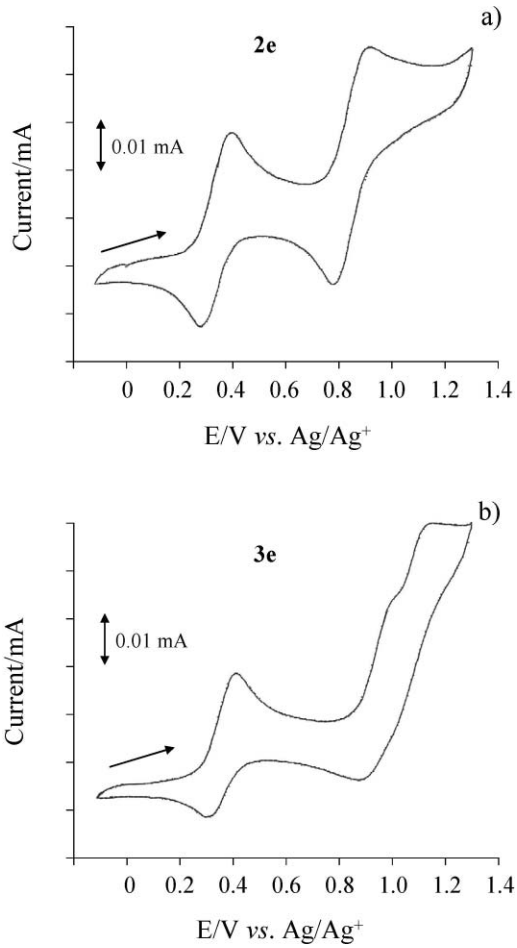

Fig. 7 Cyclic voltammograms of (a) **2e** and (b) **3e** in acetonitrile containing 0.1 M Et_4NClO_4 at a scan rate of 50 mV s^{-1}. The arrow denotes the direction of the potential scan.

the other hand, ill-defined waves for the second and third oxidation processes indicate that the second and third oxidized states of the dyes are less stable than the first ones.

The HOMO and LUMO energy levels of these dyes were evaluated from the spectral analyses and CVs.[12] They are summarized in Fig. 8a. The HOMO energy levels for **2a–f** and **3a–f** are evaluated to be *ca.* –5.50 eV with respect to vacuum level

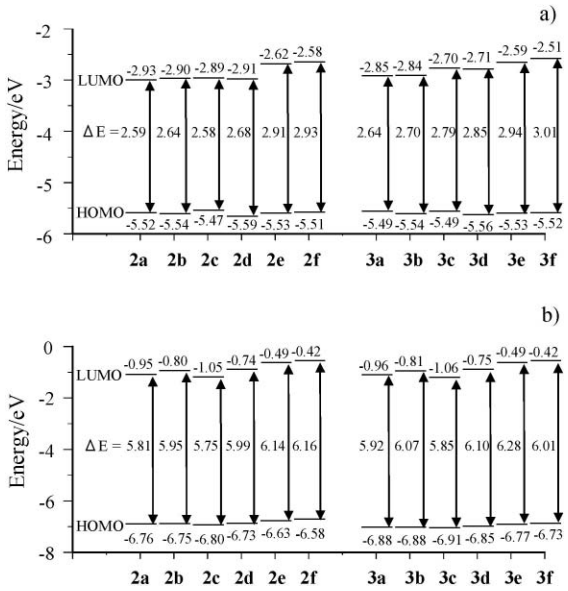

Fig. 8 (a) The HOMO and LUMO energy levels diagram for **2a–f** and **3a–f** evaluated from the absorption and fluorescence spectra and cyclic voltammograms. (b) The HOMO and LUMO energy levels diagram for **2a–f** and **3a–f** calculated by the INDO/S method *in vacuo* for **2a–f** and **3a–f**.

(Table 5). Consequently, the HOMO energy levels of the isomers **2a–f** and **3a–f** resemble very well each other, and the effect of *p*-substituted phenyl groups on the HOMO energy levels of both **2a–f** and **3a–f** was negligible. On the other hand, the LUMO energy levels of **2a–f** and **3a–f** are estimated from the oxidation potential and an intersection of absorption and fluorescence spectra corresponding to the energy gap between HOMO and LUMO corresponding to the 0–0 transition ($E_{0\text{-}0}$). The LUMO energy levels of **2a–f** are lowered in the order of **2f** (–2.58 eV) > **2e** (–2.62 eV) > **2c** (–2.89 eV) > **2b** (–2.90 eV) > **2d** (–2.91 eV) > **2a** (–2.93 eV), showing that increasing the electron-accepting ability of *p*-substituted phenyl groups lowers the LUMO energy levels of **2a–f**. Similar to **2a–f**, the lowering of LUMO energy levels in **3a–f**, which are dependent on the electron-accepting ability, were observed. These results demonstrated that in both **2a–f** and **3a–f**, increasing the electron-accepting ability of *p*-substituted phenyl groups lowers the LUMO energy levels, which lead to the decrease of energy gap between the HOMO and LUMO responsible for the red-shift of ICT absorption bands for both **2a–f** and **3a–f**.

Semi-empirical MO calculations (AM1, INDO/S)

The photophysical and electrochemical properties of the compounds **2a–f** and **3a–f** were analyzed by using semi-empirical molecular orbital (MO) calculations. The molecular structures were optimized by using the MOPAC/AM1 method,[13] and then the INDO/S method[14] using the SCRF Onsager Model was used for spectroscopic calculations in cyclohexane, 1,4-dioxane, THF and acetone, as well as that *in vacuo*. The calculated torsion angles between the *p*-substituted phenyl groups and the oxazole ring of **2a–f** and **3a–f** were *ca.* 0°. The calculated absorption wavelengths and the transition characters of the absorption bands are collected in Tables 6 and 7. The calculated absorption wavelengths and the oscillator strength values of **2a–f** and **3a–f**

Table 5 HOMO and LUMO energy levels obtained from semi-empirical molecular orbital (MO) calculations and estimated from experimental data for **2a–f** and **3a–f**

Compound	HOMO/eV[a]	LUMO/eV[a]	HOMO/eV[b]	LUMO/eV[b]	HOMO/eV[c]	LUMO/eV[c]
2a	−6.76	−0.95	−6.76	−1.02	−5.52	−2.93
2b	−6.75	−0.80	−6.73	−0.86	−5.54	−2.90
2c	−6.80	−1.05	−6.78	−1.15	−5.47	−2.89
2d	−6.73	−0.74	−6.74	−0.79	−5.59	−2.91
2e	−6.63	−0.49	−6.64	−0.49	−5.53	−2.62
2f	−6.58	−0.42	−6.59	−0.41	−5.51	−2.58
3a	−6.88	−0.96	−6.87	−1.02	−5.49	−2.85
3b	−6.88	−0.81	−6.85	−0.86	−5.54	−2.84
3c	−6.91	−1.06	−6.88	−1.15	−5.49	−2.70
3d	−6.85	−0.75	−6.84	−0.78	−5.56	−2.71
3e	−6.77	−0.49	−6.77	−0.47	−5.53	−2.59
3f	−6.73	−0.42	−6.73	−0.40	−5.52	−2.51

[a] Calculated at the INDO/S method *in vacuo*. [b] Calculated at the INDO/S method in 1,4-dioxane. [c] HOMO energy levels with respect to vacuum level are derived by the oxidation potential from the CVs (see Experimental section). LUMO energy levels are estimated from the oxidation potential and an intersection of absorption and fluorescence spectra corresponding to the energy gap between HOMO and LUMO corresponding to the 0–0 transition ($E_{0\text{-}0}$).

are comparable to the observed spectra in solution. The red-shifts of the longest excitation bands are dependent on the electron-accepting ability of *p*-substituted phenyl groups, which is in good agreement with experimental absorption results. The calculation also demonstrates that the longest excitation bands in solvents are red-shifted compared to those *in vacuo*.

For all the solvents used, the calculations indicate that the longest excitation bands (Ex1) for both isomers **2a–f** and **3a–f** are mainly assignable to the transition from the HOMO to the LUMO, where HOMO is mostly localized on the 3-dibutylamino-benzofuro[2,3-*c*]oxazolocarbazole moiety and the LUMO is mostly localized on the *p*-substituted phenyl groups. As an example, the HOMO and LUMO of **2a**, **2d**, **2f**, **3a**, **3d**, and **3f** are shown in Fig. 9a. The changes in the calculated electron density accompanying the first electron excitation for **2a–f** and **3a–f** are shown in Fig. 9b, which reveal a strong migration of an electron from the 3-dibutylamino-benzofuro[2,3-*c*]oxazolocarbazole moiety to the *p*-substituted phenyl groups in all the dyes. In the longest excitation bands, the oscillator strengths (*f*) of isomers **2a–f** are rather larger than those of isomers **3a–f**, in good agreement with the experimental ICT absorption bands. The calculations also reveal that a strong intramolecular charge transfer from the donor moiety to the acceptor moiety for **2a–f** with the conjugated linkage of the dibutylamino group to *p*-substituted phenyl groups leads to intense ICT absorption and fluorescence properties. As mentioned above, the values of the dipole moment in the ground state (μ_g) increase in the order of **2e** (1.47 D) < **2e** (1.65 D) < **2d** (3.28 D) < **2a** (5.12 D) < **2b** (6.03 D) < **2c** (7.18 D) for **2a–f**, and **3e** (1.84 D) < **3f** (2.42 D) < **3d** (3.29 D) < **3a** (5.28 D) < **3b** (6.00 D) < **3c** (6.19 D) for **3a–f**. The μ_g values of **3a–f** are lager than those of **2a–f**. The differences in the dipole moments ($\Delta\mu$) between the dipole moments of the first excited (HOMO→LUMO) and the ground states increase in the order of **2f** (5.76 D) < **2e** (6.83 D) < **2b** (10.23 D) < **2d** (10.26 D) < **2a** (11.90 D) < **2c** (12.87 D) for **2a–f**, and **3f** (5.66 D) < **3e** (6.22 D) < **3d** (8.61 D) < **3b** (8.83 D) < **3a** (10.39 D) < **3c** (11.43 D) for **3a–f**. Thus, these calculations indicate that both isomers **2a–f** and **3a–f** have similarly large dipole moments in their excited states, which explains well our finding that the fluorophores **2a–f** and **3a–f** show a large bathochromic shift of their fluorescence maxima in polar solvents and that the Stokes shift values for both isomers **2a–f** and **3a–f** in polar solvents are much larger than those in non-polar solvents. The calculations also reveal that increasing the electron-accepting ability of *p*-substituted phenyl groups, both the μ_g and the $\Delta\mu$ values of **2a–f** and **3a–f** increase, but the degree of increase in the $\Delta\mu$ value is significantly large compared to that in the μ_g value, which is responsible for the observed red-shift of

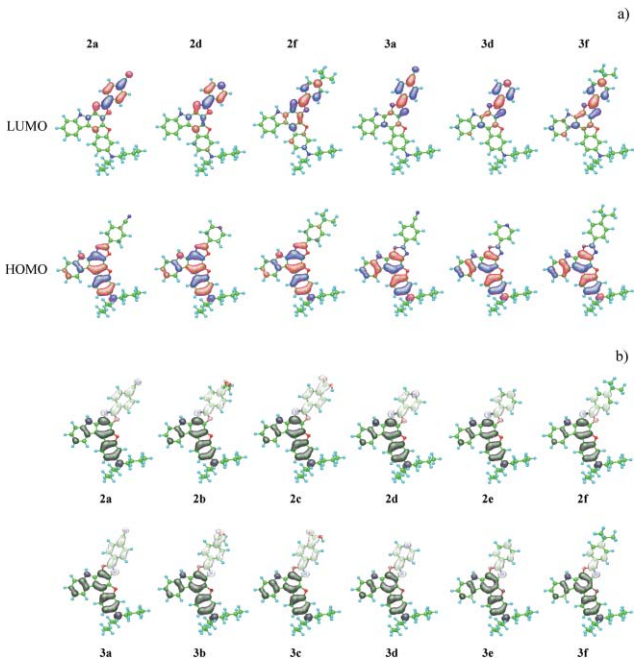

Fig. 9 (a) HOMO and LUMO electron densities of **2a**, **2d**, **2f**, **3a**, **3d** and **3f**. The red and blue lobes denote the positive and negative signs of the coefficients of the molecular orbitals. The size of each lobe is proportional to the MO coefficient. (b) Calculated electron density changes accompanying the first electronic excitation of **2a-f** and **3a-f**. The black and white lobes signify decrease and increase in electron density accompanying the electronic transition, respectively. Their areas indicate the magnitude of the electron density change (light blue, green, blue and red balls correspond to hydrogen, carbon, nitrogen, and oxygen atoms, respectively.

Table 6 Calculated absorption spectral data for **2a–f**

Compound	Solvent		Absorption (calc.) λ_{max}/nm	f^a	CI component[b]	μ/D[c]	$\Delta\mu$/D[a]
2a	No (*in vacuo*)	Ex1	400	0.95	HOMO→LUMO(77%)	5.21	11.90
		Ex2	328	0.61	HOMO→LUMO+1(45%)		3.81
	Cyclohexane	Ex1	425	0.88	HOMO→LUMO(77%)	5.40	12.94
		Ex2	331	0.63	HOMO→LUMO+1(48%)		4.36
	1,4-Dioxane	Ex1	425	0.88	HOMO→LUMO(77%)	5.42	12.98
		Ex2	331	0.64	HOMO→LUMO+1(48%)		4.34
	THF	Ex1	436	0.85	HOMO→LUMO(77%)	5.97	14.14
		Ex2	333	0.66	HOMO→LUMO+1(51%)		4.91
	Acetone	Ex1	437	0.85	HOMO→LUMO(77%)	6.13	14.45
		Ex2	333	0.66	HOMO→LUMO+1(51%)		5.09
2b	No (*in vacuo*)	Ex1	393	0.89	HOMO→LUMO(78%)	6.03	10.23
		Ex2	326	0.57	HOMO→LUMO+1(41%)		3.38
	1,4-Dioxane	Ex1	412	0.85	HOMO→LUMO(78%)	6.47	11.35
		Ex2	329	0.60	HOMO→LUMO+1(44%)		3.85
	Acetone	Ex1	422	0.81	HOMO→LUMO(78%)	7.09	12.83
		Ex2	331	0.64	HOMO→LUMO+1(46%)		4.61
2c	No (*in vacuo*)	Ex1	403	0.92	HOMO→LUMO(75%)	7.18	12.87
		Ex2	329	0.59	HOMO→LUMO+1(43%)		4.15
	1,4-Dioxane	Ex1	438	0.83	HOMO→LUMO(74%)	7.82	14.30
		Ex2	331	0.57	HOMO→LUMO+1(41%)		4.41
	Acetone	Ex1	458	0.79	HOMO→LUMO(74%)	8.78	16.27
		Ex2	338	0.64	HOMO→LUMO+1(41%)		5.78
2d	No (*in vacuo*)	Ex1	391	0.84	HOMO→LUMO(80%)	3.28	10.26
		Ex2	326	0.58	HOMO→LUMO+1(43%)		3.53
	1,4-Dioxane	Ex1	407	0.80	HOMO→LUMO(80%)	3.55	10.95
		Ex2	328	0.60	HOMO→LUMO+1(44%)		3.78
	Acetone	Ex1	412	0.79	HOMO→LUMO(80%)	3.94	11.89
		Ex2	329	0.63	HOMO→LUMO+1(47%)		4.16
2e	No (*in vacuo*)	Ex1	383	0.87	HOMO→LUMO(77%)	1.47	6.83
		Ex2	323	0.51	HOMO→LUMO+1(34%)		2.60
	1,4-Dioxane	Ex1	386	0.86	HOMO→LUMO(77%)	1.54	6.70
		Ex2	324	0.51	HOMO→LUMO+1(34%)		2.60
	Acetone	Ex1	385	0.86	HOMO→LUMO(77%)	1.64	6.51
		Ex2	324	0.51	HOMO→LUMO+1(33%)		2.60
2f	No (*in vacuo*)	Ex1	382	0.91	HOMO→LUMO(77%)	1.65	5.76
		Ex2	323	0.50	HOMO→LUMO+1(32%)		2.08
	Cyclohexane	Ex1	384	0.90	HOMO→LUMO(77%)	1.75	5.49
		Ex2	323	0.50	HOMO→LUMO+1(32%)		2.03
	1,4-Dioxane	Ex1	384	0.90	HOMO→LUMO(77%)	1.75	5.48
		Ex2	323	0.50	HOMO→LUMO+1(32%)		2.03
	THF	Ex1	383	0.90	HOMO→LUMO(76%)	1.87	5.16
		Ex2	323	0.50	HOMO→LUMO+1(31%)		1.97
	Acetone	Ex1	383	0.90	HOMO→LUMO(76%)	1.90	5.07
		Ex2	323	0.50	HOMO→LUMO+1(31%)		1.95

[a] Oscillator strength. [b] The transition is shown by an arrow from one orbital to another, followed by its percentage CI (configuration interaction) component. [c] Dipole moment in the ground state. [d] The difference in the dipole moment between the excited and the ground states

ICT absorption bands with the increase of the electron-accepting ability of *p*-substituted phenyl groups.

In the second absorption band (Ex2) for **3a–f** (HOMO − 1→LUMO), the changes in the calculated electron density accompanying the first electron excitation are a migration of an electron from the carbazole moiety to the *p*-substituted phenyl groups, which correspond to the shoulder of the observed absorption spectra. On the other hand, the differences in the dipole moments ($\Delta\mu$) between the second excited (Ex2) for **2a–f** or the third excited (Ex3) for **3a–f** (HOMO→LUMO + 1) and the ground states are 2.08–4.15 D for **2a–f** and 2.31–3.98 D for **3a–f**, where a moderate migration of charge transfer from the 3-dibutylamino-benzofuro[2,3-*c*]oxazolocarbazole moiety to the *p*-substituted phenyl groups is also observed in all the dyes. The $\Delta\mu$ values between the Ex2 for **2a–f** or the Ex3 for **3a–f** and the ground states are smaller than the $\Delta\mu$ values between the Ex1 for **2a–f** and **3a–f** and the ground states. The oscillator strengths for the second excited band for **2a–f** are rather smaller than those for the third excited band for **3a–f**, which is also in good agreement with the experimental absorption band ascribed to the $\pi\rightarrow\pi^*$ transition.

The calculated HOMO and LUMO energy levels for **2a–f** and **3a–f** *in vacuo* and in 1,4-dioxane, which is the solvent used to estimate experimentally the energy gap between HOMO and LUMO, are listed in Table 5. The calculated HOMO and LUMO energy levels in 1,4-dioxane are almost the same as those *in vacuo*, showing that the solvation effect on HOMO and LUMO energy levels is almost negligible. The calculated HOMO and LUMO energy levels diagram *in vacuo* is shown in Fig. 8b. As expected, the HOMO energy levels of both **2a–f** and **3a–f** resemble very well each other, and the effect of *p*-substituted phenyl groups on the

Table 7 Calculated absorption spectral data for **3a–f**

Compound	Solvent		Absorption (calc.) λ_{max}/nm	f[a]	CI component[b]	μ/D[c]	$\Delta\mu$/D[d]
3a	No (*in vacuo*)	Ex1	386	0.22	HOMO→LUMO(57%)	5.28	10.39
		Ex2	360	0.69	HOMO-1→LUMO(64%)		7.32
		Ex3	333	1.00	HOMO→LUMO+1(67%)		3.18
	Cyclohexane	Ex1	405	0.23	HOMO→LUMO(59%)	5.32	11.59
		Ex2	370	0.66	HOMO-1→LUMO(66%)		8.31
		Ex3	335	0.99	HOMO→LUMO+1(69%)		3.27
	1,4-Dioxane	Ex1	406	0.23	HOMO→LUMO(59%)	5.34	11.65
		Ex2	370	0.66	HOMO-1→LUMO(66%)		8.36
		Ex3	335	0.99	HOMO→LUMO+1(69%)		3.28
	THF	Ex1	415	0.25	HOMO→LUMO(62%)	5.84	13.04
		Ex2	376	0.63	HOMO-1→LUMO(68%)		9.59
		Ex3	335	0.95	HOMO→LUMO+1(69%)		3.40
	Acetone	Ex1	416	0.25	HOMO→LUMO(62%)	5.98	13.42
		Ex2	376	0.63	HOMO-1→LUMO(69%)		9.94
		Ex3	335	0.94	HOMO→LUMO+1(69%)		3.46
3b	No (*in vacuo*)	Ex1	382	0.17	HOMO→LUMO(56%)	6.00	8.83
		Ex2	356	0.62	HOMO-1→LUMO(62%)		5.95
		Ex3	331	1.00	HOMO→LUMO+1(66%)		3.48
	1,4-Dioxane	Ex1	396	0.17	HOMO→LUMO(58%)	6.38	9.87
		Ex2	363	0.61	HOMO-1→LUMO(64%)		6.86
		Ex3	333	1.00	HOMO→LUMO+1(67%)		3.55
	Acetone	Ex1	404	0.19	HOMO→LUMO(60%)	6.91	11.42
		Ex2	367	0.60	HOMO-1→LUMO(67%)		8.22
		Ex3	334	1.00	HOMO→LUMO+1(65%)		3.72
3c	No (*in vacuo*)	Ex1	389	0.22	HOMO→LUMO(57%)	6.19	11.43
		Ex2	362	0.66	HOMO-1→LUMO(63%)		8.28
		Ex3	336	0.83	HOMO→LUMO+1(51%)		2.31
	1,4-Dioxane	Ex1	415	0.23	HOMO→LUMO(59%)	6.73	12.95
		Ex2	376	0.63	HOMO-1→LUMO(66%)		9.61
		Ex3	336	0.59	HOMO→LUMO+1(40%)		1.04
	Acetone	Ex1	430	0.24	HOMO→LUMO(61%)	7.53	15.25
		Ex2	385	0.61	HOMO-1→LUMO(70%)		11.61
		Ex3	339	0.84	HOMO→LUMO+1(47%)		4.05
3d	No (*in vacuo*)	Ex1	382	0.13	HOMO→LUMO(57%)	3.29	8.61
		Ex2	354	0.55	HOMO-1→LUMO(62%)		6.21
		Ex3	331	1.00	HOMO→LUMO+1(66%)		3.98
	1,4-Dioxane	Ex1	394	0.13	HOMO→LUMO(58%)	3.55	9.23
		Ex2	360	0.54	HOMO-1→LUMO(64%)		6.84
		Ex3	333	1.00	HOMO→LUMO+1(68%)		3.84
	Acetone	Ex1	397	0.15	HOMO→LUMO(60%)	3.91	10.15
		Ex2	363	0.54	HOMO-1→LUMO(66%)		7.73
		Ex3	334	1.00	HOMO→LUMO+1(70%)		3.68
3e	No (*in vacuo*)	Ex1	375	0.12	HOMO→LUMO(51%)	1.84	6.22
		Ex2	350	0.56	HOMO-1→LUMO(53%)		3.39
		Ex3	329	1.00	HOMO→LUMO+1(60%)		3.83
	1,4-Dioxane	Ex1	377	0.12	HOMO→LUMO(51%)	1.97	6.09
		Ex2	351	0.56	HOMO-1→LUMO(62%)		3.32
		Ex3	329	1.00	HOMO→LUMO+1(60%)		3.71
	Acetone	Ex1	376	0.11	HOMO→LUMO(62%)	2.16	5.90
		Ex2	351	0.55	HOMO-1→LUMO(69%)		3.19
		Ex3	329	1.00	HOMO→LUMO+1(69%)		3.57
3f	No (*in vacuo*)	Ex1	373	0.13	HOMO→LUMO(50%)	2.42	5.66
		Ex2	351	0.61	HOMO-1→LUMO(53%)		2.62
		Ex3	329	1.00	HOMO→LUMO+1(60%)		3.17
	Cyclohexane	Ex1	374	0.13	HOMO→LUMO(49%)	2.60	5.41
		Ex2	351	0.61	HOMO-1→LUMO(52%)		2.40
		Ex3	329	1.00	HOMO→LUMO+1(60%)		3.03
	1,4-Dioxane	Ex1	374	0.13	HOMO→LUMO(49%)	2.61	5.40
		Ex2	351	0.61	HOMO-1→LUMO(52%)		2.40
		Ex3	329	1.00	HOMO→LUMO+1(60%)		3.02
	THF	Ex1	373	0.12	HOMO→LUMO(48%)	2.81	5.11
		Ex2	351	0.61	HOMO-1→LUMO(50%)		2.16
		Ex3	329	1.00	HOMO→LUMO+1(59%)		2.85
	Acetone	Ex1	372	0.12	HOMO→LUMO(48%)	2.87	5.04
		Ex2	351	0.61	HOMO-1→LUMO(49%)		2.10
		Ex3	329	1.00	HOMO→LUMO+1(59%)		2.80

[a] Oscillator strength. [b] The transition is shown by an arrow from one orbital to another, followed by its percentage CI (configuration interaction) component. [c] Dipole moment in the ground state. [d] The difference in the dipole moment between the excited and the ground states.

HOMO energy levels of both **2a–f** and **3a–f** is negligible. On the other hand, the LUMO energy levels of **2a–f** are lowered in the order of **2f**, **3f** (–0.42 eV, –0.42 eV) > **2e**, **3e** (–0.49 eV, –0.49 eV) > **2d**, **3d**(–0.74 eV, –0.75 eV) > **2b**, **3b** (–0.80 eV, –0.81 eV) > **2a**, **3a** (–0.95 eV, –0.96 eV) > **2c**, **3c** (–1.05 eV, –1.06 eV), showing that increasing the electron-accepting ability of *p*-substituted phenyl groups, lowers the LUMO energy levels of **2a–f** and **3a–f**, which is in good agreement with the experimental results (Table 5 and Fig. 8a). Consequently, it was found that the lowering of the LUMO energy levels with the increase of the electron-accepting ability leads to the decrease of energy gap between the HOMO and LUMO responsible for the longest excitation bands for both **2a–f** and **3a–f**, in qualitative agreement with experimental ICT absorption bands and electrochemical results.

Conclusion

We have designed and synthesized heteropolycyclic D–π-A structural isomers of benzofuro[2,3-*c*]oxazolo[4,5-*a*]carbazole-type (**2a–f**) and benzofuro[2,3-*c*]oxazolo[5,4-*a*]carbazole-type fluorescent dyes (**3a–f**), which differ in the position of oxygen and nitrogen atoms of the oxazole ring. Their photophysical and electrochemical properties have been investigated also. The absorption spectra of **2a–f** and **3a–f** are nearly independent of solvent polarity, while the fluorophores **2a–c** and **3a–c** having strong electron-withdrawing substituents showed a large bathochromic shift of fluorescence maxima and decrease in the fluorescence quantum yields (Φ) with increasing solvent polarity (*i.e.*, positive fluorescence solvatochromism). From the Lippert–Mataga correlation, the fluorescent dyes **2a–c** have the very large μ_e, indicating significant ICT characteristics in the excited state. Therefore, increasing of the solvent polarity stabilizes the ICT excited state relative to the ground state, resulting in large bathochromic shifts of fluorescence maxima for **2a–c**. The Strickler–Berg relations show that the low Φ_f values for **2a–f** and **3a–f** in non-polar solvents such as cyclohexane are attributed to non-radiative decay which is accelerated by an inter-system crossing (ISC) channel leading to the formation of a triplet state (T_1). For the cases of **2a–c** in 1,4-dioxane, the ^{1}ICT state is formed in high yield, leading to an increase in Φ_f and τ_f values. In highly polar solvents, the predominant species in the excited state is the TICT state, leading to the decreases of Φ_f, τ_f, and k_r values. On the other hand, for **2e**, **2f**, **3e**, and **2f** without electron-withdrawing substituents, the molecular structural changes are very small, so that the TICT state is not important at all. Therefore, the ^{1}ICT state for **2e**, **2f**, **3e**, and **2f** is stabilized in polar solvents, which is responsible for the relatively high Φ_f and τ_f values in polar solvents. Consequently, it was concluded that with increasing in solvent polarity, the predominant excited state for the D–π-A fluorescent dyes with the stronger electron-withdrawing substituents change form the ^{1}ICT state to the TICT state, which leads to the decreases of Φ_f, τ_f, and k_r values in polar solvents. However, the ^{1}ICT state for fluorescent dyes without electron-withdrawing substituents is stabilized in polar solvents, which is responsible for the high Φ_f and τ_f values in polar solvents. Furthermore, we found that the less donor–acceptor π-conjugated fluorescent dyes **3a–f** prefer the TICT state to the ^{1}ICT state, compared to **2a–f**, which have more enhanced conjugation system. The semi-empirical molecular orbital (MO) calculations revealed that stronger ICT absorption and fluorescence bands for **2a–f**, which was attributed to that the degree of donor–acceptor π-conjugation for **2a–f** is larger than that for **3a–f** owing to the conjugated linkage of the dibutylamino group to *p*-substituted phenyl group in **2a–f**. In both **2a–f** and **3a–f**, increasing of the electron-accepting ability lowers the LUMO energy levels, which lead to the decrease of energy gap between the HOMO and LUMO responsible for the red-shift of ICT absorption bands for both **2a–f** and **3a–f**.

To sum up this work, we demonstrated that the photophysical and electrochemical properties related to the ICT characteristics of the heteropolycyclic D–π-A fluorescent dyes are significantly dependent on the electron-accepting groups and donor–acceptor π-conjugation system. Therefore, new useful information concerning the ICT characteristics of heteropolycyclic D–π-A fluorescent dyes has been obtained.

Experimental

Melting points were measured with a Yanaco micro melting point apparatus MP model. IR spectra were recorded on a Perkin Elmer Spectrum One FT-IR spectrometer by ATR method. Cyclic voltammograms (CVs) were recorded in acetonitrile–Et_4NClO_4 (0.1 M) solution or DMF–Et_4NClO_4 (0.1 M) solution with a three-electrode system consisting of Ag/Ag^+ as reference electrode, Pt plate as working electrode, and Pt wire as counter electrode, by using a Hokuto Denko HAB-151 potentiostat equipped with a functional generator. Elemental analyses were recorded on a Perkin Elmer 2400 II CHN analyzer. Mass spectral data were acquired on a JEOL double-focusing mass spectrometer SX102A equipped with a FAB inlet system. ^{1}H NMR spectra were recorded on a JNM-LA-400 (400 MHz) FT NMR spectrometer with tetramethylsilane (TMS) as an internal standard. Column chromatography was performed on silica gel (KANTO CHEMICAL, 60 N, spherical, neutral). Absorption spectra were observed with a Shimadzu UV-3150 spectrophotometer and fluorescence spectra were measured with a Hitachi F-4500 spectrophotometer. The fluorescence quantum yields (Φ) were determined by a Hamamatsu C9920-01 equipped with CCD by using a calibrated integrating sphere system (λ_{ex} = 325 nm). Fluorescence lifetimes were determined with a HAMAMATSU Photonics C4334/C8898 time-resolved spectrophotometer by excitation at 375 nm (laser diode). that follow headings should not be indented).

Preparation of 7-(4-cyanophenyl)-3-dibutylamino-benzofuro[2,3-*c*]oxazolo[4,5-*a*]carbazole (2a) and 7-(4-cyanophenyl)-3-dibutylamino-benzofuro[2,3-*c*]oxazolo[5,4-*a*]carbazole (3a)

A solution of **1** (1.00 g, 2.41 mmol), *p*-cyanobenzaldehyde (0.32 g, 2.41 mmol), and ammonium acetate (3.72 g, 48 mmol) in acetic acid (30 ml) was stirred at 90 °C for 1 h. After the reaction was completed, the reaction mixture was poured into water. The resulting precipitate was filtered, washed with water and dried. The residue was chromatographed on silica gel (toluene–acetic acid = 5 : 1 as eluent) to give **2a** (0.70 g, yield 55%) as an orange powder and **3a** (0.20 g, yield 16%) as an orange powder; **2a**: mp. 295–296 °C; ^{1}H NMR (acetone-d_6, TMS): δ = 1.03 (6H, t), 1.47-1.52 (4H, m), 1.70-1.78 (4H, m), 3.54 (4H, t), 7.02-7.08 (2H, m), 7.41-7.44 (1H, m), 7.51-7.55 (1H, m), 7.80 (1H, d, J = 8.28 Hz), 8.06 (2H, d, J = 8.56 Hz), 8.51 (2H, d, J = 8.56 Hz), 8.55 (1H,

d, $J = 8.76$ Hz), 8.71 (1H, d, $J = 8.04$ Hz), 11.49 ppm (1H, s, -NH). IR (KBr): $\tilde{\nu} = 3427$, 2227 cm^{-1}. Elemental analysis calcd (%) for $C_{34}H_{30}N_4O_2$ (526.63): C 77.54, H 5.74, N 10.64; found: C 77.51, H 5.71, N 10.60; **3a**: decomposition 303–304 °C; ^{1}H NMR (acetone-d_6, TMS): $\delta = 1.03$ (6H, t), 1.46-1.52 (4H, m), 1.70-1.78 (4H, m), 3.52 (4H, t), 7.01 (1H, dd, $J = 2.20$ and 9.04 Hz), 7.07 (1H, d, $J = 2.20$ Hz), 7.43 (1H, m), 7.54 (1H, m), 7.76 (1H, d, $J = 8.20$ Hz), 8.06 (2H, d, $J = 8.32$ Hz), 8.50 (2H, d, $J = 8.32$ Hz), 8.51 (1H, d, $J = 9.04$ Hz), 8.74 (1H, d, $J = 7.80$ Hz), 11.49 ppm (1H, s, -NH). IR (KBr): $\tilde{\nu} = 3341$, 2229 cm^{-1}. Elemental analysis calcd (%) for $C_{34}H_{30}N_4O_2$ (526.63): C 77.54, H 5.74, N 10.64; found: C 77.48, H 5.51, N 10.51.

Preparation of 7-(4-methoxycarbonylphenyl)-3-dibutylamino-benzofuro[2,3-*c*]oxazolo[4,5-*a*]carbazole (2b) and 7-(4-methoxycarbonylphenyl)-3-dibutylamino-benzofuro[2,3-*c*]oxazolo[5,4-*a*]carbazole (3b)

A solution of **1** (0.20 g, 0.48 mmol), 4-formyl-benzoic acid methyl ester (0.08 g, 0.48 mmol) and ammonium acetate (1.20 g, 15 mmol) in acetic acid (35 ml) was stirred at 90 °C for 1 h. After the reaction was complete, the reaction mixture was condensed. The resulting precipitate was washed with water and dried. The residue was chromatographed on silica gel (dichloromethane–hexane = 5 : 1 as eluent) to give **2b** (0.16 g, yield 58%) as an orange powder and **3b** (0.08 g, yield 29%) as an orange powder; **2b**: mp. 284–285 °C; ^{1}H NMR (DMSO-d_6, TMS) $\delta = 1.00$ (6H, t), 1.39-1.45 (4H, m), 1.61-1.66 (4H, m), 3.23-3.51 (4H, m) (overlapping peak of dissolved water in DMSO-d_6), 3.94 (3H, s), 6.99 (1H, dd, $J = 1.96$, 8.80 Hz), 7.08 (1H, d, $J = 1.96$ Hz), 7.40 (1H, t), 7.52 (1H, t), 7.69 (1H, d, $J = 7,84$ Hz), 8.26 (2H, d, $J = 8.80$ Hz), 8.44 (2H, d, $J = 8.80$ Hz), 8.49 (1H, d, $J = 8.80$ Hz), 8.63 (1H, d, $J = 8.80$ Hz), 12.53 ppm (1H, s, -NH). IR (ATR): $\tilde{\nu} = 3361$, 1705 cm^{-1}. FABMS $m/z = 559$ (M$^+$); **3b**: mp. 273–275 °C; ^{1}H NMR (DMSO-d_6, TMS) $\delta = 1.00$ (6H, t), 1.44 (4H, m), 1.65 (4H, m), 3.25-3.51 (4H, m), (overlapping peak of dissolved water in DMSO-d_6), 3.94 (3H, s), 6.97 (1H, d, $J = 8.76$), 7.07 (1H, s), 7.41 (1H, t), 7.55 (1H, t), 7.72 (1H, d, $J = 7.80$ Hz), 8.28 (2H, d, $J = 7.80$ Hz), 8.46 (2H, d, $J = 7.80$ Hz), 8.48 (1H, d, $J = 7.84$), 8.66 (1H, d, $J = 7.84$), 11.51 ppm (1H, s, -NH). IR (ATR): $\tilde{\nu} = 3214$, 1699 cm^{-1}. FABMS $m/z = 559$ (M$^+$).

Preparation of 7-(4-carboxyphenyl)-3-dibutylamino-benzofuro[2,3-*c*]oxazolo[4,5-*a*]carbazole (2c) and 7-(4-carboxyphenyl)-3-dibutylamino-benzofuro[2,3-*c*]oxazolo[5,4-*a*]carbazole (3c)

A solution of **1** (0.50 g, 1.21 mmol), 4-formyl-benzoic acid (0.18 g, , 1.21 mmol) and ammonium acetate (2.79 g, 36.1 mmol) in acetic acid (70 ml) was stirred at 90 °C for 1.5 h. After the reaction was complete, the reaction mixture was condensed. The resulting precipitate was washed with water and dried. The residue was chromatographed on silica gel (dichloromethane–hexane = 5 : 1 as eluent) to give **2c** (0.22 g, yield 33%) as a dark orange powder and **3c** (0.05 g, yield 5%) also as an orange powder; **2c**: mp. 296–297 °C; ^{1}H NMR (DMSO-d_6, TMS) $\delta = 1.00$ (6H, t), 1.39-1.46 (4H, m), 1.60-1.67 (4H, m), 3.23-3.65 (4H, m) (overlapping peak of dissolved water in DMSO-d_6), 6.99 (1H, dd, $J = 1.96$, 8.80 Hz), 7.08 (1H, d, $J = 1.96$), 7.40 (1H, t), 7.51 (1H, t), 7.70 (1H, d, $J = 7.80$ Hz), 8.22 (2H, d, $J = 7.84$), 8.39 (2H, d, $J = 7.84$), 8.50 (1H, d, $J = 8.76$ Hz), 8.64 (1H, d, $J = 7.84$), 12.50 ppm (1H, s, -NH). IR (ATR): $\tilde{\nu} = 3240$, 1692 cm^{-1}. Elemental analysis calcd (%) for $C_{34}H_{31}N_3O_4$: C 74.84, H 5.73, N 7.70; found: C 74.72, H 5.63, N 7.67. FABMS $m/z = 545$ (M$^+$); **3c**: mp. 280–282 °C; ^{1}H NMR (DMSO-d_6, TMS) $\delta = 1.06$ (6H, t), 1.44-1.52 (4H, m), 1.67-1.73 (4H, m), 3.20-3.55 (4H, m) (overlapping peak of dissolved water in DMSO-d_6), 7.02 (1H, dd, $J = 1.96$ and 8.76 Hz), 7.14 (1H, d, $J = 1.96$ Hz), 7.47 (1H, t), 7.60 (1H, t), 7.78 (1H, d, $J = 8.80$ Hz), 8.32 (2H, d, $J = 8.80$ Hz), 8.49 (2H, d, $J = 7.84$ Hz), 8.53 (1H, d, $J = 8.80$ Hz), 8.72 (1H, d, $J = 7.84$ Hz), 12.53 ppm (1H, s, -NH). IR (ATR): $\tilde{\nu} = 3214$, 1699 cm^{-1}. FABMS m / $z = 545$ (M$^+$)

Preparation of 7-(4-pyridyl)-3-dibutylamino-benzofuro[2,3-*c*]oxazolo[4,5-*a*]carbazole (2d) and 7-(4-pyridyl)-3-dibutylamino-benzofuro[2,3-*c*]oxazolo[5,4-*a*]carbazole (3d)

A solution of **1** (0.20 g, 0.48 mmol), *p*-cyanobenzaldehyde (0.052 g, 0.48 mmol), and ammonium acetate (0.75 g, 9.73 mmol) in acetic acid (50 ml) was stirred at 90 °C for 2 h. After concentrating under reduced pressure, the resulting residue was chromatographed on silica gel (toluene–acetic acid = 5 : 1 as eluent) to give **2d** (0.074 g, yield 31%) as an orange powder and **3d** (0.031 g, yield 12%) as an orange powder; **2d**: mp. 256–258 °C; ^{1}H NMR (acetone-d_6, TMS) $\delta = 1.03$ (6H, t), 1.46-1.51 (4H, m), 1.70-1.76 (4H, m), 3.54 (4H, t), 7.04 (1H, dd, $J = 1.96$ and 8.00 Hz), 7.07 (1H, d, $J = 1.96$ Hz), 7.42 (1H, t), 7.53 (1H, t), 7.82 (1H, d, $J = 8.00$ Hz), 8.23 (2H, d, $J = 6.80$ Hz), 8.58 (1H, d, $J = 8.00$ Hz), 8.74 (1H, d, $J = 8.00$ Hz), 8.90 (2H, d, $J = 6.80$ Hz), 11.55 ppm (1H, s, -NH). IR (ATR): $\tilde{\nu} = 3061$, 1624, 1602 cm^{-1}. FABMS $m/z = 503$ (M$^+$); **3d**: mp. 264–266 °C; ^{1}H NMR (DMSO-d_6, TMS) $\delta = 1.00$ (6H, t), 1.39-1.46 (4H, m), 1.60-1.67 (4H, m), 3.20-3.48 (4H, m) (overlapping peak of dissolved water in DMSO-d_6), 6.96 (2H, dd, $J = 2.20$ and 8.00 Hz), 7.09 (1H, d, $J = 2.20$ Hz), 7.43 (1H, t), 7.54 (1H, t), 7.73 (1H, d, $J = 8.00$ Hz), 8.20 (2H, d), 8.48 (1H, d, $J = 8.80$ Hz), 8.66 (1H, d, $J = 8.80$ Hz), 8.93 (2H, d), 11.55 ppm (1H, s, -NH). IR (ATR): $\tilde{\nu} = 3095$, 1602, 1559 cm^{-1}. FABMS $m/z = 503$ (M$^+$).

Preparation of 7-phenyl-3-dibutylamino-benzofuro[2,3-*c*]oxazolo[4,5-*a*]carbazole (2e) and 7-phenyl-3-dibutylamino-benzofuro[2,3-*c*]oxazolo[5,4-*a*]carbazole (3e)

A solution of **1** (0.30 g, 0.72 mmol), benzaldehyde (0.08 g, 0.72 mmol) and ammonium acetate (1.67 g, 21.7 mmol) in acetic acid (40 ml) was stirred at 90 °C for 1 h. After concentrating under reduced pressure, the resulting residue was purified by chromatography on silica gel (dichloromethane–hexane = 7 : 1 as eluent) to give **2e** (0.31 g, yield 52%) as a light yellow powder and **3e** (0.10 g, yield 17%) also as a light yellow powder; **2e**: mp. 197–198 °C; ^{1}H NMR (acetone-d_6, TMS) $\delta = 1.03$ (6H, t), 1.46-1.52 (4H, m), 1.70-1.76 (4H, m), 3.53 (4H, t), 7.03 (1H, dd, $J = 1.96$ and 8.80 Hz), 7.06 (1H, d, $J = 1.96$ Hz), 7.40 (1H, t), 7.51 (1H, t), 7.67 (3H, m), 7.81 (1H, d, $J = 7.80$ Hz), 8.38 (2H, dd, $J = 1.96$ and 7.80 Hz), 8.56 (1H, d, $J = 8.80$ Hz), 8.72 (1H, d, $J = 7.84$ Hz), 11.42 ppm (1H, s, -NH). IR (ATR): $\tilde{\nu} = 3572$, 1623 cm^{-1}. FABMS $m/z = 501$ (M$^+$); **3e**: mp. 174–175 °C; ^{1}H NMR (acetone-d_6, TMS) $\delta = 1.03$ (6H, t), 1.46-1.52 (4H, m), 1.69-1.74 (4H, m), 3.52 (4H, t), 7.02 (1H, dd, $J = 1.96$ and 8.76 Hz), 7.08 (1H, d, $J = 1.96$ Hz, 7.44 (1H, t), 7.53 (1H, t), 7.66 (3H, m), 7.78 (1H, d, $J = 8.80$ Hz), 8.37 (2H, dd, $J = 2.92$ and 6.84), 8.52 (1H, d, $J = 8.80$ Hz), 8.74

(1H, d, $J = 8.80$ Hz), 11.35 (1H, s, -NH). IR (ATR): $\tilde{\nu} = 3428$, 1620 cm^{-1}. FABMS $m/z = 501$ (M$^+$).

Preparation of 7-(4-*tert*-butylphenyl)-3-dibutylamino-benzofuro[2,3-*c*]oxazolo[4,5-*a*]carbazole (2f) and 7-(4-*tert*-butylphenyl)-3-dibutylamino-benzofuro[2,3-*c*]oxazolo[5,4-*a*]carbazole (3f)

A solution of **1** (0.40 g, 0.72 mmol), 4-*tert*-butylbenzaldehyde (0.12 g, 0.72 mmol) and ammonium acetate (1.66 g, 21.5 mmol) in acetic acid (25 ml) was stirred at 90 °C for 1.5 h. After the reaction was complete, the reaction mixture was condensed. The resulting precipitate was washed with water and dried. The residue was chromatographed on silica gel (dichloromethane–hexane = 7 : 1 as eluent) to give **2f** (0.11 g, 26%) as a light yellow powder and **3f** (0.03 g, 7%) as a light yellow powder; **2f**: mp. 233–236 °C; ^{1}H NMR (acetone-d_6, TMS) $\delta = 1.04$ (6H, t), 1.28 (9H, s), 1.48-1.54 (4H, m), 1.70-1.78 (4H, m), 3.55 (4H, t), 7.04-7.10 (2H, m), 7.41-7.45 (1H, m), 7.64-7.70 (1H, m), 7.80 (2H, d, $J = 8.56$ Hz), 8.29 (1H, d, $J = 7.80$ Hz), 8.53 (1H, d, $J = 8.80$ Hz), 8.70 (1H, d, $J = 5.84$ Hz), 11.49 ppm (1H, s, -NH). IR (ATR): $\tilde{\nu} = 3397$, 1623 cm^{-1}; elemental analysis calcd (%) for $C_{37}H_{39}N_3O_2$ (557.30): calcd. C 79.68, H 7.05, N, 7.53, found C 79.71, H 7.24, N 7.45. EIMS $m/z = 557$ (M$^+$); **3f**: mp. 207–210 °C; ^{1}H NMR (acetone-d_6, TMS) $\delta = 1.03$ (6H, t), 1.25 (9H, s), 1.47-1.54 (4H, m), 1.69-1.78 (4H, m), 3.52 (4H, t), 6.98-7.01 (1H, dd, $J = 8.80$ Hz and 2.92 Hz), 7.07 (1H, m, $J = 2.92$ Hz), 7.36-7,43 (1H, m), 7.50-7.53 (1H, m), 7.72 (2H, d, $J = 7.84$ Hz), 7.76 (1H, d, $J = 7.80$ Hz), 8.30 (2H, d, $J = 8.76$ Hz), 8.51 (1H, d, $J = 8.76$ Hz), 8.73 (1H, d, $J = 7.80$ Hz), 11.35 ppm (1H, s, -NH). IR (ATR): $\tilde{\nu} = 3211$, 1620 cm^{-1}. FABMS $m/z = 557$ (M$^+$).

Estimation of the HOMO and LUMO energy levels for the compounds[12]

The energy value for Ag/Ag$^+$ with respect to the vacuum level is estimated as −5.16 eV, determined from −4.6 eV for the standard electrode potential $E°$ of a normal hydrogen electrode (NHE) on the vacuum level, and 0.56 V for Ag/Ag$^+$ *vs*. NHE. Therefore, the HOMO and LUMO energy levels for the compounds were obtained through eqn (5) and (6) as follows:

$$\text{HOMO} = -(E^{ox} + 5.16)\ \text{eV} \quad (5)$$

$$\text{LUMO} = -[E_{0\text{-}0} - (E^{ox} + 5.16)]\ \text{eV} \quad (6)$$

in which E^{ox} and $E_{0\text{-}0}$ are the oxidation potential *vs*. Ag/Ag$^+$ and an intersection of absorption and fluorescence spectra corresponding to the energy gap between HOMO and LUMO.

Computational methods

The semi-empirical calculations were carried out with the Win-MOPAC Ver. 3.9 package (Fujitsu, Chiba, Japan). Geometry calculations in the ground state were made using the AM1 method.[13] All geometries were completely optimized (keyword PRECISE) by the eigenvector following routine (keyword EF). Experimental absorption spectra of the compounds were compared with their absorption data by the semi-empirical method INDO/S (intermediate neglect of differential overlap/spectroscopic)[14] using the SCRF Onsager Model. All INDO/S calculations were performed using single excitation full SCF/CI (self-consistent field/configuration interaction), which includes the configuration with one electron excited from any occupied orbital to any unoccupied orbital, where 225 configurations were considered [keyword CI (15 15)].

Acknowledgements

This work was supported by Grants-in-Aid for Scientific Research (B) (19350094) and for Young Scientist (B) (20750161) from the Japan Society for the Promotion of Science (JSPS), by Mitsubishi Chemical Corporation Fund, and by a research grant from Kinki Invention Center.

References

1 (*a*) K. Hara, T. Sato, R. Katoh, A. Furude, Y. Ohga, A. Shinpo, S. Suga, K. Sayama, H. Sugihara and H. Arakawa, *J. Phys. Chem. B*, 2003, **107**, 597; (*b*) K. Hara, Z.-S. Wang, T. Sato, A. Furube, R. Katoh, H. Sugihara, Y. Dan-oh, C. Kasada, A. Shinpo and S. Suga, *J. Phys. Chem. B*, 2005, **109**, 15476; (*c*) K. Hara, T. Sato, R. Katoh, A. Furube, T. Yoshihara, M. Murai, M. Kurashige, S. Ito, A. Shinpo, S. Suga and H. Arakawa, *Adv. Funct. Mater.*, 2005, **15**, 246; (*d*) R. Chen, X. Yang, H. Tian, X. Wang, A. Hagfeldt and L. Sun, *Chem. Mater.*, 2007, **19**, 4007; (*e*) T. Edvinsson, C. Li, N. Pschirer, J. Schöneboom, F. Eickemeyer, R. Sens, G. Boschloo, A. Herrmann, K. Müllen and A. Hagfeldt, *J. Phys. Chem. C*, 2007, **111**, 15137; (*f*) Z.-S. Wang, Y. Cui, K. Hara, Y. Dan-oh, C. Kasada and A. Shinpo, *Adv. Mater.*, 2007, **19**, 1138; (*g*) H. Choi, C. Baik, S. O. Kang, J. Ko, M.-S. Kang, M. K. Nazeeruddin and M. Grätzel, *Angew. Chem., Int. Ed.*, 2008, **47**, 327; (*h*) S. Kim, D. Kim, H. Choi, M.-S. Kang, K. Song, S. O. Kang and J. Ko, *Chem. Commun.*, 2008, 4951; (*i*) W.-H. Liu, I.-C. Wu, C.-H. Lai, C.-H. Lai, P.-T. Chou, Y.-T. Li, C.-L. Chen, Y.-Y. Hsu and Y. Chi, *Chem. Commun.*, 2008, 5152.

2 (*a*) Y. Ooyama, Y. Shimada, Y. Kagawa, I. Imae and Y. Harima, *Org. Biomol. Chem.*, 2007, **5**, 2046; (*b*) Y. Ooyama, Y. Shimada, Y. Kagawa, Y. Yamada, I. Imae, K. Komaguchi and Y. Harima, *Tetrahedron Lett.*, 2007, **48**, 9167; (*c*) Y. Ooyama, A. Ishii, Y. Kagawa, I. Imae and Y. Harima, *New J. Chem.*, 2007, **31**, 2076; (*d*) D. P. Hagberg, J.-H. Yum, H. Lee, F. D. Angelis, T. Marinado, K. M. Karlsson, R. Humphry-Baker, L. Sun, A. Hagfeldt, M. Grätzel and M. K. Nazeeruddin, *J. Am. Chem. Soc.*, 2008, **130**, 6259; (*e*) B. Liu, W. Zhu, Q. Zhang, W. Wu, M. Xu, Z. Ning, Y. Xie and H. Tian, *Chem. Commun.*, 2009, 1766; (*f*) G. Li, Y.-F. Zhou, X.-B. Cao, P. Bao, K.-J. Jiang, Y. Lin and L.-M. Yang, *Chem. Commun.*, 2009, 2201; (*g*) Y. Ooyama, Y. Shimada, A. Ishii, G. Ito, Yu. Kagawa, I. Imae, K. Komaguchi and Y. Harima, *J. Photochem. Photobiol., A*, 2009, **203**, 177; (*h*) Y. Ooyama and Y. Harima, *Eur. J. Org. Chem.*, 2009, 2903; (*i*) H. Choi, I. Raabe, D. Kim, F. Teocoli, C. Kim, K. Song, J.-H. Yum, J. Ko, Md. K. Nazeeruddin and M. Grätzel, *Chem.–Eur. J.*, 2010, **16**, 1193; (*j*) Y. Ooyama, S. Inoue, R. Asada, G. Ito, K. Kushimoto, K. Komaguchi, I. Imae and Y. Harima, *Eur. J. Org. Chem.*, 2010, **1**, 92.

3 (*a*) H.-C. Yeh, L.-H. Chan, W.-C. Wu and C.-T. Chen, *J. Mater. Chem.*, 2004, **14**, 1293; (*b*) C.-T. Chen, *Chem. Mater.*, 2004, **16**, 4389; (*c*) G. Hughes and M. R. Bryce, *J. Mater. Chem.*, 2005, **15**, 94; (*d*) S.-L. Lin, L.-H. Chan, R.-H. Lee, M.-Y. Yen, W.-J. Kuo, C.-T. Chen and R.-J. jeng, *Adv. Mater.*, 2008, **20**, 3947; (*e*) G. Qian, Z. Zhong, M. Luo, D. Yu, Z. Zhang, Z. Y. Wang and D. Ma, *Adv. Mater.*, 2009, **21**, 111.

4 (*a*) K. Köller, *Appl. Fluorescence Technol.*, 1989, **1**, 1; (*b*) K. Yoshida, Y. Ooyama, H. Miyazaki and S. Watanabe, *J. Chem. Soc., Perkin Trans. 2*, 2002, 700; (*c*) Y. Ooyama, T. Nakamura and K. Yoshida, *New J. Chem.*, 2005, **29**, 447; (*d*) J. N. Wilson and U. H. F. Bunz, *J. Am. Chem. Soc.*, 2005, **127**, 4124; (*e*) Y. Ooyama, T. Okamoto, Y. Yamaguchi, T. Suzuki, A. Hayashi and K. Yoshida, *Chem.–Eur. J.*, 2006, **12**, 7827; (*f*) Y. Ooyama, S. Yoshikawa, S. Watanabe and K. Yoshida, *Org. Biomol. Chem.*, 2006, **4**, 3406; (*g*) L. Xue, C. Liu and H. Jiang, *Chem. Commun.*, 2009, 1061; (*h*) W. Jiang and W. Wang, *Chem. Commun.*, 2009, 3913; (*i*) M. H. Kim, H. H. Jang, S. Yi, S.-K. Chang and M. S. Han, *Chem. Commun.*, 2009, 4838; (*j*) F. Qian, C. Zhang, Y. Zhang, W. He, X.

Gao, P. Hu and Z. Guo, *J. Am. Chem. Soc.*, 2009, **131**, 1460; (*k*) R. Guliyev, A. Coskun and E. U. Akkaya, *J. Am. Chem. Soc.*, 2009, **131**, 9007.
5 (*a*) B. Valeur, *Molecular Fluorescence*, VCH, Weinheim, 2002; (*b*) C. Reichardt, *Solvents and Solvent Effects in Organic Chemistry*, VCH, Weinheim, 2003; (*c*) H. Zollinger, *Color Chemistry*, VCH, Weinheim, 2003.
6 (*a*) D. S. Tyson, E. F. Fabrizo, M. J. Panzner, J. D. Kinder, J.-P. Buisson, J. B. Christensen and M. A. Meador, *J. Photochem. Photobiol., A*, 2005, **172**, 97; (*b*) F. B. Dias, S. Pollock, G. Hedley, L.-O. Pålsson, A. Monkman, I. I. Perepichka, I. F. Perepichka, M. Tavasli and M. R. Bryce, *J. Phys. Chem. B*, 2006, **110**, 19329; (*c*) M.-J. R. P. Queiroz, A. S. Abreu, E. M. S. Castanheira and P. M. T. Ferreira, *Tetrahedron*, 2007, **63**, 2215; (*d*) S. L. Bondarev, S. A. Tikhomirov, V. N. Knyukshto, A. A. Turban, A. A. Ishchenko, A. V. Kulinich and I. Ledoux, *J. Lumin.*, 2007, **124**, 178; (*e*) F. Han, L. Chi, W. Wu, X Liang, M. Fu and J. Zhao, *J. Photochem. Photobiol., A*, 2008, **196**, 10; (*f*) G.-J. Zhao, R.-K. Chen, M.-T. Sun, J.-Y. Liu, G.-Y. Li, Y.-L. Gao, K.-L. Han, X.-C. Yang and L. Sun, *Chem.–Eur. J.*, 2008, **14**, 6935; (*g*) S. Pramanik, P. Banerjee, A. Sarkar, A. Mukherjee, K. K. Mahalanabis and S. C. Bhattacharya, *Spectrochim. Acta Part A*, 2009, **71**, 1327; (*h*) J. Hashemi and N. Alizadeh, *Spectrochim. Acta, Part A*, 2009, **73**, 121; (*i*) P. Song, S.-G. Sun, J.-Y. Liu, Y.-Q. Xu, K.-L. Han and X.-J. Peng, *Spectrochim. Acta, Part A*, 2009, **74**, 753; (*j*) S. Achelle, I. Nouira, B. Pfaffinger, Y. Ramondenc, N. Plé and J. R. López, *J. Org. Chem.*, 2009, **74**, 3711; (*k*) K. Fujimoto, H. Shimizu, M. Furusyo, S. Akiyama, M. Ishida, U. Furukawa, T. Yokoo and M. Inoue, *Tetrahedron*, 2009, **65**, 9357; (*l*) C. Aronica, A. Venancio-Marques, J. Chauvin, V. Robert and G. Lemercier, *Chem.–Eur. J.*, 2009, **15**, 5047; (*m*) R. S. Butler, P. Cohn, P. Tenzel, K. A. Abboud and R. K. Castellano, *J. Am. Chem. Soc.*, 2009, **131**, 623.
7 (*a*) Y. Ooyama and Y. Harima, *Chem. Lett.*, 2006, **35**, 902; (*b*) Y. Ooyama, Y. Kagawa and Y. Harima, *Eur. J. Org. Chem.*, 2007, 3613.
8 (*a*) S. Sumalekshmy and K. R. Gopidas, *J. Phys. Chem. B*, 2004, **108**, 3705; (*b*) S. Sumalekshmy and K. R. Gopidas, *New J. Chem.*, 2005, **29**, 325; (*c*) S. Sumalekshmy and K. R. Gopidas, *Photochem. Photobiol. Sci.*, 2005, **4**, 539.
9 (*a*) E. Lippert, *Z. Naturforsch. Part A*, 1955, **10**, 541; (*b*) N. Mataga, Y. Kaifu and M. Koizumi, *Bull. Chem. Soc. Jpn.*, 1956, **29**, 465.
10 S. J. Strickler and R. A. Berg, *J. Chem. Phys.*, 1962, **37**, 814.
11 (*a*) B. Cohen, C. E. Crespo-Hernández and B. Kohler, *Faraday Discuss.*, 2004, **127**, 137; (*b*) J. Mohanty and W. M. Nau, *Photochem. Photobiol. Sci.*, 2004, **3**, 1026; (*c*) G. Angulo, G. Grampp, J. Grilj, P. Jacques, S. Landgraf and A. Rosspeintner, *J. Photochem. Photobiol., A*, 2008, **199**, 204; (*d*) L. O'Neill, P. Lynch, M. McNamara and H. J. Byrne, *Polymer*, 2008, **49**, 4109.
12 (*a*) J. Pommerehne, H. Vestweber, W. Guss, R. Mahrt, H. Bässler, M. Porsch and J. Daub, *Adv. Mater.*, 1995, **7**, 551; (*b*) V. A. Montes, R. Pohl, J. Shinar and P. Anzenbacher, Jr, *Chem.–Eur. J.*, 2006, **12**, 4523.
13 M. J. S. Dewar, E. G. Zoebisch, E. F. Healy and J. J. Stewart, *J. Am. Chem. Soc.*, 1985, **107**, 3902.
14 (*a*) J. E. Ridley and M. C. Zerner, *Theor. Chim. Acta*, 1973, **32**, 111; (*b*) J. E. Ridley and M. C. Zerner, *Theor. Chim. Acta*, 1976, **42**, 223; (*c*) A. D. Bacon and M. C. Zerner, *Theor. Chim. Acta*, 1979, **53**, 21; (*d*) H. A. Kurtz, J. J. P. Stewart and D. M. Dieter, *J. Comput. Chem.*, 1990, **11**, 82.

